QUILL

Quarterly Reports

August - October 2019

Contents

QUILL Quarterly Report

August 2019 – October 2019

Name:	**Marian Borucki**		
Supervisor(s):	Prof Peter Nockemann, Dr Stephen Glover and Dr Małgorzata Swadźba-Kwaśny		
Position:	PhD Student		
Start date:	01.2018	Anticipated end date:	
Funding body:	Bryden Centre, Horiba Mira		

Lithium Ion Batteries Degradation Study Using Spectroscopy Techniques

Background

Lithium ion batteries (LIB) are secondary (rechargeable) batteries that are currently the main energy storage device. LIBs are applied in various applications as in portable devices, grid energy storage, grid current regulation as well as in hybrid- and electric vehicles. Energy harvested by the renewable energies is often dependent on the environment, which results in discontinuous energy supply. In order to store excess energy that has been generated during times where lower amounts of energy are consumed within a day, energy storage stations based on LIB are used. The other, yet not less important application for LIBs is replacing the fossil fuel by storing the energy in the transport sector, namely in hybrid (HEV) and electric vehicles (EV). The trend of replacing the fossil fuels both in energy sector by supplementing them with renewable energy power plants as well as by supporting the market of HEV, EV and fuel-cell vehicles (FCEV) is growing. New policies of EV30@30 and *New Policy Scenario* are the programmes that are aimed towards expanding the market of HEV, EV and FCEV, thus the supply for lithium ion batteries will grow. The Automotive Council UK has in their roadmap reports on lithium ion batteries that have gathered up the issues that need to be addressed if the automotive of EV, HEV and FCEV is to grow. Such issues are based on the need for improving the safety of battery usage, lowering the costs of the batteries, researching new materials for the batteries that will allow to store more energy and provide more power, thus be fast chargeable. Issues concerning the battery pack and modules combination, minimisation of the losses related to cell joining, their thermal management, increasing the lifespan of the batteries as well as increasing their recyclability, therefore, require further research towards the next generation of batteries.

In order to meet all the requirements a thorough study of the current battery technology as well as the development of a new chemistries is needed. Lifespan and the safety of the battery is of very high importance when it comes to the battery application in the transportation market. Battery life is limited by the degradation mechanism that occur inside the cell. Currently there is a known number of such mechanisms occurring, even though the proper investigating techniques allowing *in operando* study have not been developed yet. Moreover, the degradation is very much chemistry dependent, so whenever the new chemistry is tested for the battery the new degradation mechanism could occur. On the other hand, the safety of the battery is limited by the usage of the organic based electrolyte, which is highly flammable and might lead to battery explosion. Proper electrolyte, which are non-toxic, environmentally friendly, non-flammable as well as of high performance should be developed. By developing the new electrolytes, often the development of

the electrodes is also needed since the electrolyte stability as well as the energy density of the battery depends highly on them.

Objective of this work

The aim of the PhD programme is focused on investigating the lithium ion battery (LIB) degradation processes occurring inside the cell during its operation. In order to achieve the goal a development of an experimental method based on the spectroscopic analytical techniques will be needed. A proper method would allow to observe and measure the changes that occur *in operando* inside the lithium ion battery. During the PhD programme an analytical data of LIB degradation will be acquired, using various analytical techniques including electrode surface examination, electrolyte composition. Acquired spectroscopy data will be linked with the rest of the data gathered in order to develop the sensing method. Eventually, batteries of a different cell chemistries will be investigated.

Progress to date

The first paragraph is devoted to summarizing previous reports, in order to maintain the continuity of the research progression. I found it also important as in the further describing the progress up to date a reference to previous reports will be done.

The studied lithium-ion electrochemical cells are a CR2032 coin (button) cell type. The chemistry of a cell is based on graphite anode and $LiNi_{8/10}Mn_{1/10}Co_{1/10}O_2$ (NMC811) as a cathode material, which are coated on the thin foil (~0.01 mm) of copper and alumina current collators, respectively. In the 'commercial' cell setup a supporting electrolyte of 1 M $LiPF_6$ is dissolved in ethylene carbonate (EC) : ethylene methylene carbonate (EMC) as 1:1 molar ratio solution with 2% vol. vinylene carbonate (VC) which is used as film-forming agent. Since the electrolyte is liquid a polyolefin separator of good ionic conductivity characteristic is needed in order to prevent the short-circuit in event of physical contact of electrodes. The assembly of Li-ion cells are undertaken in a glovebox, with inert atmosphere (Ar based) and low concentration of water and oxygen (less than 0.1 ppm) due to the use of an organic electrolyte. The 'commercial' lithium-ion cell scheme both as a technical inscription and graphitic representation can be observed in Figure 1.

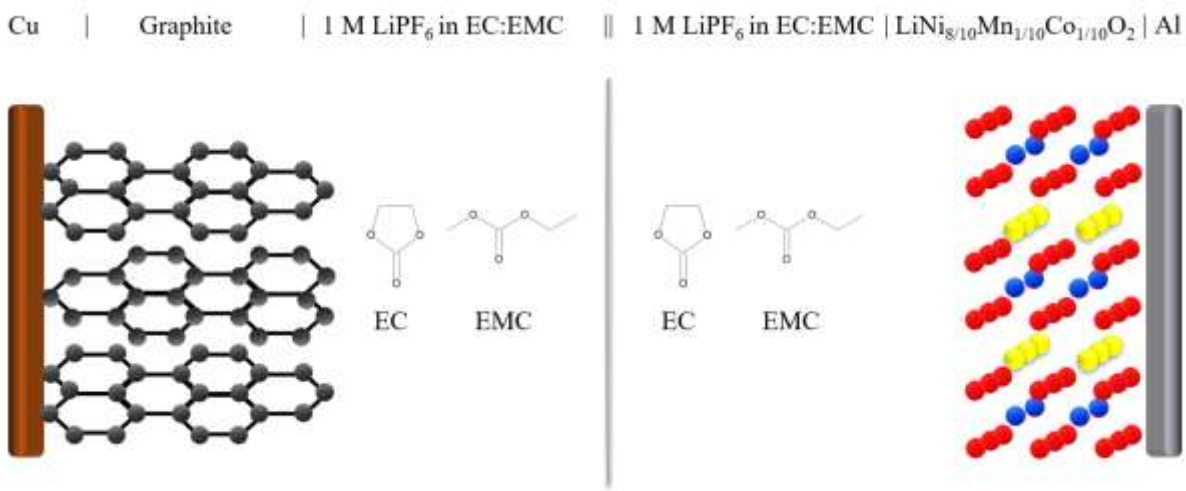

Figure 1 *Lithium-ion cell inscription and scheme.*

In the above figure, individual parts of the studied cell can be distinguished, from the left to the right: a copper current collector, graphite anode, electrolyte separated by the polyolefin film,

NMC811 as cathode material and alumina current collector. All these cell components are arranged in the same pattern inside the studied samples.

Further to the assembly process of lithium-ion batteries, their quality control and testing procedures are implemented. Four procedures can be distinguished, each with different purpose. These procedures are:

a) Three charge-discharge cycles at theoretical 0.1 C current rate – establishing the properties of the cell
b) Four series of three cycles with varying current rates – studying the cell stability in various current rates
c) Single discharge with varying current – performing control of the power characteristics of the cell
d) Dynamic stress testing (DST) cycles – performing the charge/discharge cycles with changing power outputs.

The Project roadmap (**Figure 2**) illustrates the actions that need to be undertaken in order to fully investigate the degradations of the lithium ion-battery.

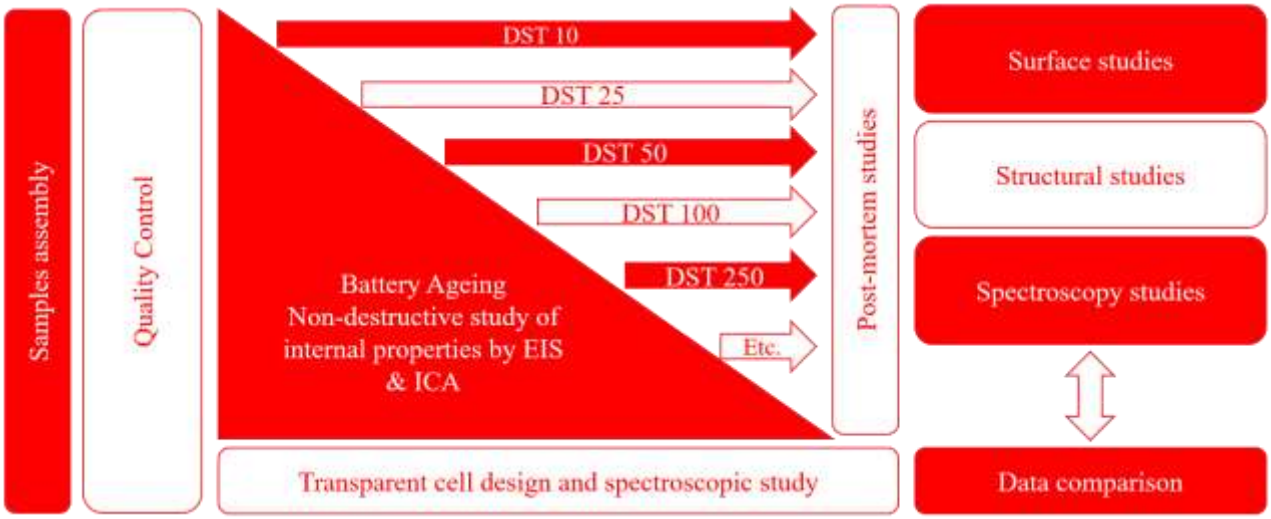

Figure 2 *Project Roadmap.*

The sample preparation and assembly is the first step. Then the quality control of all samples is undertaken in order to reject the samples that do not meet the requirements. Only the samples that are considered to be stable are further studied by cycling them according to DST procedure. The study of degradation needs to be performed considering the wide-angle of cell properties, and they are summarised in three categories as shown in **Figure 3**.

As it can be seen in the degradation study scheme, three types of study need to be undertaken. Firstly, a study that allows to monitor and investigate the change in the internal properties of the lithium ion cell, such as its voltage response to current, power outputs, capacity etc. need to be conducted. Such studies include electrochemical impedance spectroscopy (EIS) and incremental capacity analysis (ICA). A huge advantage of the internal properties study is the fact that they are non-destructive methods. At it can be seen in **Figure 2**, both ICA and EIS are performed together with dynamic stress testing (DST) procedure. An internal property study is followed by both studies

of chemistry and structure, yet in opposition to ICA and EIS, these studies are not only invasive but also needed to be performed post-mortem, so a disassembly of a lithium-ion cell is needed. Disassembly is performed at different stages of battery life (number next to DST). As one can see simultaneously to standard sample ageing a transparent coin cell design of a sample is undertaken in order to perform spectroscopic studies *ex situ, in operando*. Data gathered from the transparent cell spectroscopy study is due to be collected, analysed and compared to one acquired from standard CR2032 samples.

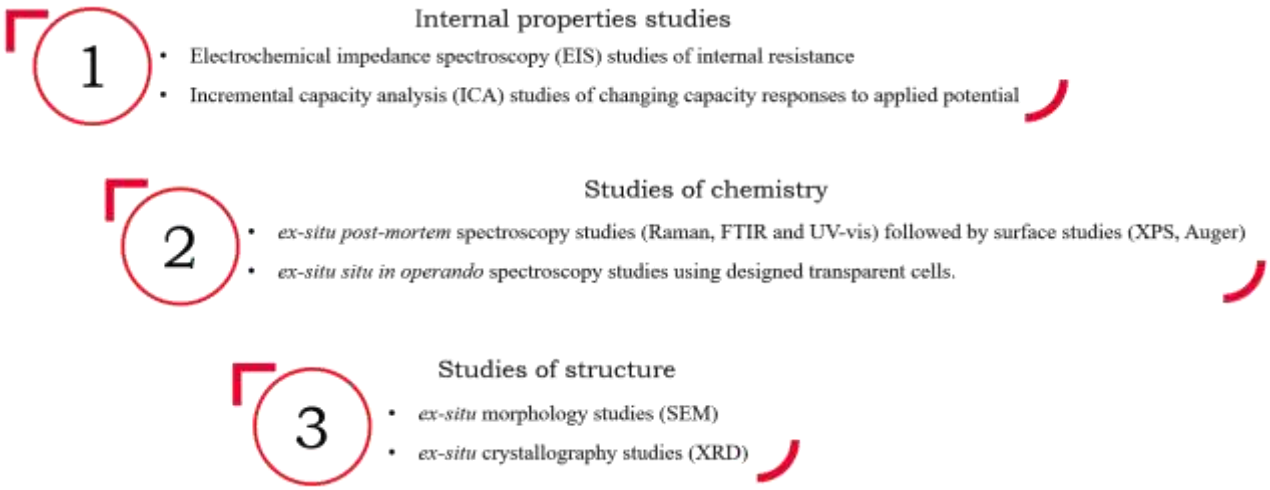

Figure 3 *Degradation studies scheme.*

Previously a number of EIS data collected was gathered at different stages of battery life from its initial charging and quality control up to 100 cycles of dynamic stress testing. Due to increased interval between studied points in battery life, only two new points were investigated in a 3 month interval - one of 250 and 500 cycles of DST. Due to that fact I would withhold a proper interpretation of new data for EIS until more points are acquired. The same as the EIS data, an ICA for a discharge curves of the samples at 250 and 500 DST stage was undertaken and it will be summarised together as more of the data points are obtained.

In the meantime, a transparent cell design was developed in order to study the changes in spectroscopic data *in operando, ex situ*. Firstly, a shape for the electrodes that will allow to study them both in the same time was developed and designed in an AutoCad, it can be seen in Figure 4. The important aspect in designing was the fact that proportions in electrode and electrolyte materials should be maintained the same both in the transparent coin cell and standard CR2032 so the data obtained from both of them would be comparable. A proper machining method for obtaining such a special electrode shape was investigated and decided to be the laser cutting. In order to properly laser cut the electrodes, the electrode material will be sandwiched between two sheets of 2mm aluminium with countersunk bolts in it in order to ensure the integrity during the cutting process.

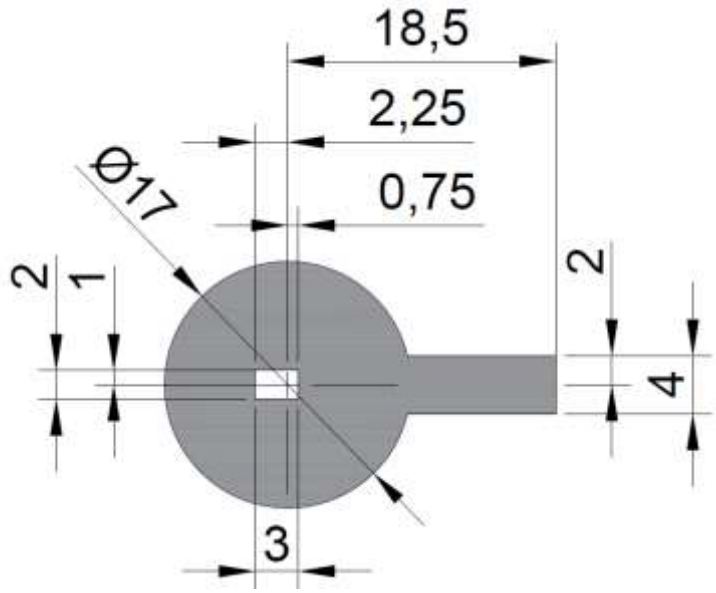

Figure 4 *Electrode shape to be used in transparent coin cell.*

One of the problems of laser cutting is the fact that laser beam of higher power could damage the edges of the electrode. That is why a laser of different powers will be used and each of cut electrode will be investigated under microscope in order to evaluate the laser influence of different powers to the material.

Conclusions and future work

Ageing tests of the manufactured batteries will be undertaken for the duration of up to 3000 cycles in order to determine the degradation mechanisms occurring inside the batteries. The internal properties study as EIS and ICA will be further implemented on 1000th, 2000th and 3000th cycle of the battery ageing procedure. At each of these points the cycled batteries will be disassembled depending on their age. *Ex situ* microscopic, crystallographic as well as spectroscopic studies will be performed in favour of obtaining the information about the severity of each degradation mechanisms. The degradation mechanisms of losses in lithium inventory (LLI) losses in active material (LAM) and Internal resistance increase will be investigated. The transparent cell will be assembled and an experiment, one that will allow to monitor the battery during its ageing will be set up. Meanwhile the methodology of *in situ* spectroscopic study of the cell will be developed. Data gathered through *ex situ, post mortem* studies will be compared to the data obtained from *ex situ, in operando* studies and further used to determine the level of degradation for the lithium ion cells monitored through *in situ in operando* technique.

Moreover, the electrochemical systems of different electrolytes and electrodes setups will be assembled and further studied according to the previous mentioned methodology. The planed studied setups include carbon, silica and carbon-silica based anodes as well as the pure and semi-solid ionic liquid electrolytes. The studies of their stability as well as overall performance will be undertaken.

QUILL Quarterly Report

August 2019 – October 2019

Name:	**Dominic Burns**		
Supervisor(s):	Prof John Holbrey and Dr Gosia Swadzba-Kwasny		
Position:	PhD Student		
Start date:	01/10/2019	Anticipated end date:	31/03/2023
Funding body:	EPSRC/Chevron		

Recycle and Reuse of Process Water Through Sulphate and Calcium Removal

Background

Water purification is essential to the modern world but in order to be most efficient with our resources we must use the correct purification method depending on the level of purity required. For example, if we were to distil all of the worlds drinking water that would be a waste of energy when an acceptable level of purity can be achieved by reverse osmosis.

High sulphate and calcium levels is an issue in many industries, some of which include metallurgy, nuclear waste, mining. Calcium sulphate causes permanent hardness in water and so can precipitate in pipes causing scaling. Many of these industries must comply with regulated discharge limits on the total dissolved solids or specific limits for sulphate or calcium.

Many different approaches to sulphate removal have been developed over the past few decades to address the issues face by industry, these can be divided into three main categories; chemical, physical and biological extraction. As well as advances in these processes, much research has also been done in synthesising molecular chemical receptors for sulphate recognition and removal.
Many of the methods used to remove sulphate (eg. SAVMIN^{TM} process and ultrafiltration to name a few) are also effective methods to remove calcium ions. Selective extraction of calcium can be difficult because of its similar properties to other metals and so, most of the existing literature describes general metal extraction, which is already a large area for ionic liquid (IL) research. Some ILs have already been developed for many different metal extractions but to date no work has been published on their ability to remove sulphate. Aisling McGuigan and Dr Syed Nasir Shah had previously been working on removing sulphate using a trihexyltetradecyl-phosphonium chloride IL for QUILL but their results were inconclusive as barium precipitation followed by gravimetric analysis is not a reliable way to quantify sulphate removal.

Objective of this work

To design a hydrophobic IL that can selectively pull sulphate ions out of an aqueous phase in the presence of competing anions during bi-phasic extraction. Then to design another IL to do the same with calcium cations.

Progress to date

To date I have been familiarising myself with the relevant literature as well as being trained on the new EDXRF machine which will allow me to precisely quantify the efficiency of the sulphate and calcium removal. To do this the EDXRF requires a supply of helium to accurately quantify sulphur which has been the major hold up so far in this process. This issue should be resolved in the next few days which will allow me to then start to produce some results. So far I have been preparing by synthesising six water immiscible tetraoctylphosphonium ILs with hydrophobic anions to test their ability to extract calcium via coordination of the anion to the metal.

Conclusions and future work

This project is still in its very early stages yet due to the length of time its taken to get EDXRF machine and its helium installed however, current literature and previous results suggest that ILs are promising candidates for effective sulphate and calcium removal.

The next step is to get the helium set up for the EDXRF and to start running small scale extractions to test the sulphate extraction ability of $[P_{66614}]Cl$ for various sulphate concentrations, phase ratios, mixing time and with competing anions. This should hopefully give us insight into the mechanism of the extraction and how to improve it.

I will also be testing the ability of various hydrophobic anions with $[P_{8888}]^+$, such as oleate, decanoate and benzoate among others for their ability to extract calcium into the IL phase before then trying to optimise the IL to be more selective for calcium.

QUILL Quarterly Report

August - October 2019

Name:	**Emily Byrne**		
Supervisor(s):	Dr Małgorzata Swadźba-Kwaśny and Prof John Holbrey		
Position:	PhD student		
Start date:	October 2017	Anticipated end date:	October 2020
Funding body:	DfE (Department for the Economy)		

Physical Characterisation of Functional Liquids

Background

It is proposed that deep eutectic solvents 'DES' are a chemical component mixture composed of hydrogen bond donors and acceptors which have intermolecular interactions that result in a freezing point which is lower than that of the isolated individual components of the system with no interactions between each other.[1] They are asymmetric species which, due to their orbitals' inability to overlap well and thus, pack into a regular lattice arrangement, have low lattice energy and so do not require a large amount of energy in order to exist as a liquid and as a result tend to have low melting points.

The most common and well renowned DES are those prepared with the combination of organic salts such as choline chloride, which act as a hydrogen bond acceptor and carboxylic acids or alcohols with a hydrogen bond donating role.[2–5] However, these solvents are generally miscible with water and so their application is quite limited. Therefore, work was undertaken by van Osch *et al.* which led to the publication of the first hydrophobic deep eutectic solvent using a carboxylic acid hydrogen bond donor and a long chain quaternary ammonium salt in 2015.[6] In addition to this, DES have since been formed using alcohols and fatty acid hydrogen bond donors in combination with organic salts to form deep eutectic solvents which can be used for extraction of metals[7] and natural products[8,9]. In addition to this, in an attempt to reduce the viscosity associated with these charged DES species, Ribeiro *et al.* developed DES systems using D-menthol and carboxylic acid hydrogen bond donors where the individual components used are non-ionic species.[10] More recently, DES made with the combination of trioctylphosphine oxide (TOPO) and phenol have been published and its use as a uranyl extractant shown.[11]

TOPO has a number of uses such as capping agents[12–16] in nanoparticle synthesis, metals[17,18], organic acids[19–22] and phenolics[23–26] extraction and so a number of DES will be prepared using a range of hydrogen bond donors most suited to the potential application.

Objective of this work

In this work, thermal decomposition pathways were studied by analysis of both the liquid and gas phase before and after holding the sample at a temperature above that of its initial thermal decomposition. Evolved gas analysis using GC-MS identified gases released during decomposition and NMR analysis of the liquid phase highlighted the species present in the bulk of the liquid. Reasoning for the inability to electrodeposit gallium has been shown by ^{71}Ga NMR studies and attempts made to recover gallium from the eutectic phase through back extraction.

Progress to date

The thermal decomposition of these TOPO:malonic acid mixtures occurs in a 2 step event, with weight loss from isothermal TGA at 90 °C (χ_{TOPO} = 0.33) confirming that malonic acid is lost first with an initial decomposition rate of 5.8% h^{-1} in the first 3 hours. Using the χ_{TOPO} = 0.33 composition held isothermally at 90 °C, analysis of the liquid and gas phases using NMR and GC-MS respectively also supported the loss of malonic acid in the first step. In addition to the pungent smell of vinegar from the decomposed sample, ^{13}C NMR highlighted the presence of acetic acid in the mixture after decomposition. GC-MS indicated the presence of a large loss of CO_2 from the sample during decomposition as well as trace amounts of CO and H_2O. These results are in agreement with the decomposition of malonic acid via a decarboxylation mechanism to produce acetic acid and carbon dioxide. [27–32]

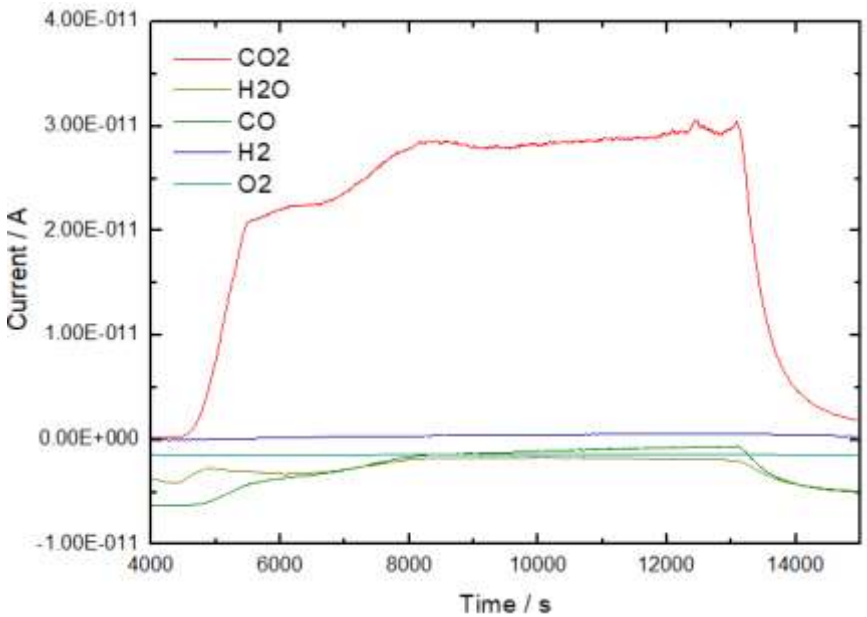

Figure 1 Evolved gas analysis during thermal decomposition of χ_{TOPO} = 0.33 TOPO:malonic acid at 90 °C using GC-MS

Trace amounts of CO released are likely as a result of the secondary decomposition of acetic acid.[33] As CO is detected, it is thought that the secondary decomposition of acetic acid also occurs primarily via a decarboxylation mechanism in this case. It was not possible to monitor the evolution of ethenone or methane in this study.

In addition to decomposition via a decarboxylation mechanism, a small amount of sublimation of malonic acid was also observed with crystallisation around the top of the round bottomed flask; confirmed as malonic acid by ^{13}C NMR. This is common in the decomposition many organic acids.[30] Solid, white particles were also isolated from the bulk of the liquid after decomposition and confirmed as malonic acid by ^{13}C NMR due to pure malonic acid crashing out of the mixture.

Isothermal TGA shows the initial rate of weight loss of TOPO:levulinic acid (χ_{TOPO} = 0.33) varies from 4.0-2.6% h^{-1} within in first 4 hours at 90 °C. Upon increasing temperature of isothermal TGA to 140 °C, initial rate of weight loss increases to 45.8-2.4% h^{-1} within the first 2 hours. Weight loss from isothermal TGA at 140 °C indicates that levulinic acid is lost first. Significant sublimation of levulinic acid occurs with the sublimed product collected at the top of the round bottomed flask and identified as levulinic acid via ^{13}C and ^{1}H NMR. Furthermore, the bulk of liquid turns yellow.

Evolved gas analysis via GC-MS indicated loss of CO_2 which increased with increasing temperature from 90-140°C. This is coherent with thermal decarboxylation of carboxylic acids in the liquid phase and the thermal decarboxylation of levulinic acid to produce butanone.[34]

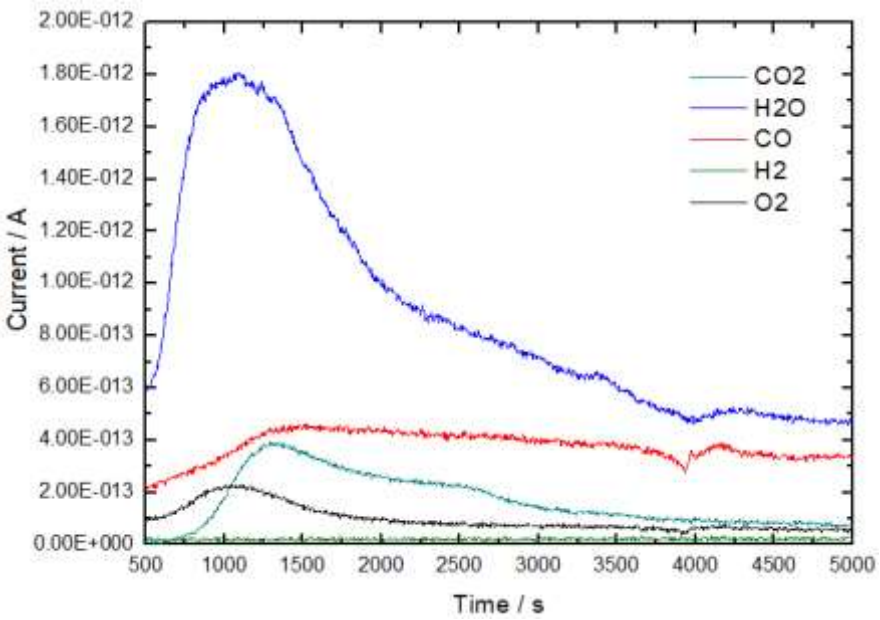

Figure 2 Evolved gas analysis during thermal decomposition of χ_{TOPO} = 0.33 TOPO:levulinic acid at 140 °C using GC-MS

However, NMR analysis of the liquid phase did not indicate the presence of butanone. This is thought to be due to its high vapour pressure and boiling point of 80 °C,[34] while samples were held isothermally at 90 °C and above. Integration of the ^{1}H spectra of the liquid phase only indicated component loss after isothermal heating at 140 °C for 1 hour.

Stripping of gallium back out of the eutectic and the speciation of gallium present in the extractant phase after extraction has also been studied. Previously, it was shown that gallium could not be electrodeposited using cyclic voltammetry. Speciation studies using ^{71}Ga NMR have now indicated that this is due to the presence of a $[GaCl_4]^-$ species present in the eutectic which is difficult to reduce. ^{71}Ga NMR highlights the presence of a single peak at 245.6 ppm in χ_{TOPO} = 0.67

TOPO:Malonic acid after extraction at 6 M HCl. This peak is in agreement with ^{71}Ga chemical shifts indicative of $[GaCl_4]^-$ present in chlorogallate ionic liquids[35,36] as well as in other solvents such as water.[37] Stripping via back extraction by changing the HCl concentration of the aqueous phase has also not been successful as shown by the table below.

Table 1 Back-extraction efficiency obtained when changing the concentration of HCl in the aqueous phase

Stripping phase	Extraction efficiency / %
H_2O	0.4
0.5 M HCl	0.3
0.5 M HCl heated to 70 °C	0.2

Conclusions and future work

To conclude, analysis of the gas and liquid phases during and after thermal decomposition respectively indicate that decarboxylation is the major route of decomposition in both the TOPO:malonic acid and TOPO:levulinic acid mixtures. For TOPO:malonic acid, evolved gas analysis indicates the release of CO2 detected by GC-MS and NMR analysis of the liquid phase highlights the presence of acetic acid after thermal decomposition; known products of malonic acid thermal decomposition via decarboxylation. Similarly, evolved gas analysis of TOPO:levulinic acid mixtures indicate the release of CO2, however, butanone – the product of decarboxylation of levulinic acid cannot be seen in the NMR spectra of the liquid phase; likely as a result of the sample being held above butanone's boiling point. In both cases sublimation of the pure acid can be seen, although this is to a much greater extent in the TOPO:levulinic acid sample.

In addition to this, $[GaCl_4]^-$ has been identified as the species of gallium present in the eutectic phase after extraction. This explains the inability to electrodeposit gallium from the extractant phase as this speciation of gallium is difficult to reduce. In addition to this, back extraction via changing the HCl concentration of the aqueous phase has been unsuccessful in recovering gallium due to back-extraction efficiencies $<1\%$.

Future work will include attempting back extraction techniques via contacting the eutectic phase post extraction with a mildly basic aqueous phase do determine if this will lead to the recovery of gallium. If this is unsuccessful, another application route for these TOPO based DESs will need to be explored.

References

1. A. P. Abbott, G. Capper, D. L. Davies, H. L. Munro, R. K. Rasheed and V. Tambyrajah, *Chem. Commun.*, 2001, 2010–2011.
2. Q. Zhang, K. De Oliveira Vigier, S. Royer and F. Jérôme, *Chem. Soc. Rev.*, 2012, **41**, 7108.
3. M. Francisco, A. van den Bruinhorst and M. C. Kroon, *Angew. Chem. Int. Ed.*, 2013, **52**, 3074–3085.
4. E. L. Smith, A. P. Abbott and K. S. Ryder, *Chem. Rev.*, 2014, **114**, 11060–11082.
5. A. P. Abbott, D. Boothby, G. Capper, D. L. Davies and R. K. Rasheed, *J. Am. Chem. Soc.*, 2004, **126**, 9142–9147.
6. D. J. G. P. van Osch, L. F. Zubeir, A. van den Bruinhorst, M. A. A. Rocha and M. C. Kroon, *Green Chem.*, 2015, **17**, 4518–4521.
7. D. J. G. P. van Osch, D. Parmentier, C. H. J. T. Dietz, A. van den Bruinhorst, R. Tuinier and M. C. Kroon, *Chem. Commun.*, 2016, **52**, 11987−11990.

8. J. Cao, M. Yang, F. Cao, J. Wang and E. Su, *ACS Sustain. Chem. Eng.*, 2017, **5**, 3270–3278.
9. J. . Cao, L. . Chen, M. . Li, F. . Cao, L. . Zhao and E. Su, *Green Chem.*, 2018, **20**, 1879−1886.
10. B. D. Ribeiro, C. Florindo, L. C. Iff, M. A. Z. Coelho and I. M. Marrucho, *ACS Sustain. Chem. Eng.*, 2015, **3**, 2469–2477.
11. M. Gilmore, É. N. Mccourt, F. Connolly, P. Nockemann, M. Swadźba-kwaśny and J. D. Holbrey, *ACS Sustain. Chem. Eng*, 2018, **6**, 17323–17332.
12. I. Mekis, D. V Talapin, A. Kornowski, M. Haase and H. Weller, *J. Phys. Chem.*, 2003, **107**, 7454–7462.
13. F. V Mikulec, M. Kuno, M. Bennati, D. A. Hall, R. G. Griffin and M. G. Bawendi, *J. Am. Chem. Soc*, 2000, **122**, 2532–2540.
14. T. Cassagneau, T. E. Mallouk and J. H. Fendler, *J. Am. Chem. Soc*, 1998, **120**, 7848–7859.
15. T. Trindade and P. O. Brien, *Chem Mater*, 1997, **9**, 523–530.
16. A. A. Guzelian, J. E. B. Katari, A. V Kadavanich, U. Banin, K. Hamad, E. Juban, A. P. Alivisatos, R. H. Wolters, C. C. Arnold and J. R. Heath, *J. Phys. Chem.*, 1996, **100**, 7212–7219.
17. T. Sato, T. Nakamura and S. Ishikawa, *Solvent Extr. Ion Exch.*, 1984, **2**, 201–212.
18. E. K. Watson and W. A. Rickelton, *Solvent Extr. Ion Exch.*, 1992, **10**, 879–889.
19. P. O. . Saboe, L. P. . Manker, W. E. . Michener, D. J. . Peterson, D. G. . Brandner, S. P. . Deutch, M. . Kumar, R. M. . Cywar, B. G. T.; and E. M. Karp, *Green Chem.*, 2018, **20**, 1791–1804.
20. T. Brouwer, M. Blahusiak, K. Babic and B. Schuur, *Sep. Purif. Technol.*, 2017, **185**, 186–195.
21. G. Kim, S. Park and B. Um, *Ind. Crop. Prod.*, 2016, **89**, 34–44.
22. S. Uenoyama, T. Hano, M. Hirata and S. Miura, *J. Chem. Technol. Biotechnol.*, 1996, **67**, 260–264.
23. P. Praveen and K. C. Loh, *Chem. Eng. J.*, 2014, **255**, 641–649.
24. P. Praveen and K. Loh, *Chemosphere*, 2016, **153**, 405–413.
25. P. Praveen and K. Loh, *J. Membr. Sci.*, 2013, **437**, 1–6.
26. E. K. Watson, W. A. Rickelton, A. J. Robertson and T. J. Brown, *Solvent Extr. Ion Exch.*, 1988, **6**, 207–220.
27. C. N. Hinshelwood, *J. Chem. Soc., Trans.*, 1920, **117**, 156–165.
28. J. Györe and M. Ecet, *J. Therm. Anal.*, 1970, **2**, 397–409.
29. A. M. El-Awad and R. M. Mahfouz, *J. Therm. Anal.*, 1989, **35**, 1413–1421.
30. W. W. Wendlandt and J. A. Hoiberg, *Anal. Chim. Acta*, 1963, **28**, 506–511.
31. S. Gál, T. Meisel and L. Erdey, *J. Therm. Anal.*, 1969, **1**, 159–170.
32. V. L. Stanford and S. Vyazovkin, *Ind. Eng. Chem. Res.*, 2017, **56**, 7964–7970.
33. P. G. Blake and G. E. Jackson, *J. Chem. Soc. B*, 1968, 1153–1155.
34. M. Grilc and B. Likozar, *Chem. Eng. J.*, 2017, **330**, 383–397.
35. C. Hardacre, A. R. W. Murphy, A. K. R. Seddon, G. Srinivasan and M. Swadzba-Kwasny, *Aust. J. Chem.*, 2010, **63**, 845–848.
36. K. R. Seddon, G. Srinivasan, Swadzba-Kwasny and A. R. Wilson, *Phys. Chem. Chem. phys.*, 2013, **15**, 4518–4526.
37. J. Mason, Ed., *Multinuclear NMR*, Springer, London, 1987.

QUILL Quarterly Report

August - October 2019

Name:	**Dr Martyn Earle**		
Supervisor(s):			
Position:	Senior Research Fellow		
Start date:	01-09-2018	Anticipated end date:	31-12-2019
Funding body:	BBSRC		

Microemulsion Solvent Systems for Bio-Separations

Background

The separation of proteins and related compounds often involves the use of aqueous biphasic solvent systems for both solvent extraction and countercurrent chromatographic separation. In this work we have developed a methodology capable of performing the separation of a two-component mixture of two proteins, which uses water as the mobile phase. A new aqueous biphasic solvent system has been developed which can selectively dissolve proteins and has been successfully tested in a centrifugal partition chromatography apparatus using a water / hydrophobic microemulsion solvent system.

Objective of this work

The objectives of the work are to develop a clean, high capacity methodology for separating peptides and proteins, using ionic liquid containing stationary phases and water as a mobile phase in countercurrent chromatography and centrifugal partition chromatography.

Progress to date

The work has developed and tested a model separation of lysozyme from cytochrome C in the CPC apparatus. The separation achieved a complete separation of the two proteins, and the research has led to the development of new water / hydrophobic microemulsion solvent systems.

Conclusions and future work

The separation of lysozyme from cytochrome C has been successfully tested and a suitable range of solvent systems designed for protein separations have been developed. The mobile phase being comprised of water (saturated with an organic solvent) contains very low levels of involatile ionic liquids, which can be solvent extracted and recycled from the aqueous solution of separated proteins emerging from the CPC apparatus. This results in the protein solution containing no other involatile materials which makes the isolation of the protein from water very simple. The future work is to optimise the lysozyme / cytochrome C separation, and test a wider range of separations.

Microemulsion Solvent Systems for Bio-Separations of Proteins

Dr Martyn Earle

28-11-2019

Introduction

The manufacture of high-value pharmaceutical products (such as peptides and proteins) require fast, low cost, reliable, GMP-compliant, scalable preparatory chromatography processes and technologies. By the use of a combination of three relatively new technologies, namely: (1) ionic liquids,[1] (2) modern high performance countercurrent chromatography (HPCCC)[2] or centrifugal partition chromatography (CPC)[3] and (3) co-solvent free, high water content microemulsions[4] (Figure 1) derived from catanionic surfactants (surface active hydrophobic ionic liquids),[5-7] we propose their combined use in enabling a new range of high performance and environmentally friendly separations of proteins and peptides. The importance and motivation for this research is that ionic liquids have been found to be excellent solvents for proteins,[10] and have been demonstrated to work in a highly effective manner in countercurrent chromatography (CCC).[9,11] Taken together, this enables peptide and protein separations to be carried out at much higher concentrations and space time yields,[12] using relatively small amounts of solvent, than is currently possible with conventionally used solvent systems.[13] Since CCC separations with ionic liquids and high water content microemulsions behave in a different manner, and have different selectivities, when compared to HPLC, gel or size exclusion chromatography, electrophoresis and other methodologies used in protein purification,[14,15] it will complement currently available technologies.[14]

Figure 1 An triphasic solvent system made from a mixture of water, hexane and a catanionic surfactant (Fig 2.) The middle microemulsion phase is 75 mol% water. The lower phase is 99.7 mol% water and 0.3 mol% hexane, and the upper phase is excess hexane.[6,7] The high-water content microemulsion (middle phase) is remarkable in that it requires no co-solvents and is termed "hydrophobic water".

This research is based on the discovery of a new "revolutionary" triphasic solvent system (Figure 1) and new biphasic water / hydrophobic microemulsion solvent systems based on ethyl ethanoate. These separations use the cheapest liquid solvent available (water) as a mobile phase and relatively cheap organic solvents such as hexane or ethyl ethanoate. The ionic liquid which has been tested is at most 1.5 mol% or 10 wt% of the stationary phase making separations economical when compares to aqueous biphasic solvent systems based of $K_2[HPO_4]$ / PEG or $K_2[HPO_4]$ / $[C_4mim]Cl$. These separations are generally tolerant of solids which would normally block or destroy a HPLC or gel chromatography column, making the CPC separations much more robust and insensitive to particulate matter often found in crude protein samples. The water / ionic liquid + organic solvent microemulsion solvent systems used in CPC separations have solute capacities of **1 to 2 order of magnitude** higher than those used in HPLC, and since the stationary phase is a liquid, rather than a surface (as in solid HPLC columns), the stationary phase can have much higher solute capacities than is found in similarly sized HPLC columns.[19] Thus, far lower quantities of solvent per gram of protein are required in CPC separations, than is the case for HPLC separations.[19] These ionic liquid and microemulsion solvent systems, combined with automated CPC apparatus and technologies have the potential to revolutionise the way in which proteins, enzymes and biopolymers are produced and dramatically reduce the production costs.

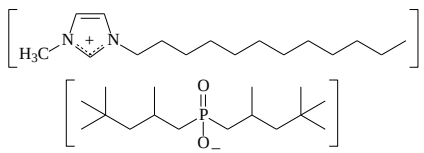

Figure 2 The structure of the microemulsion forming ionic liquid $[C_{12}mim][DiIOP]$, which is used to form the "hydrophobic water phase" in Figure 1.

In liquid-liquid chromatography (LLC, HPCCC and CPC), a solute or analyte is partitioned between two liquid phases, where one phase is a mobile phase (MP) and one phase is a stationary phase (SP) (Fig. 3). The

distribution ratio (K_D) of a solute between the two phases where K_D = $[Solute]_{SP}/[Solute]_{MP}$ determines the elution rate of the solute. Thus, in LLC, biphasic solvent systems are chosen or designed that give values of K_D in the 0.5 to 3.0 range. For many bio-molecules which are water soluble, aqueous biphasic solvent (ABS) systems are commonly used, which are comprised of two immiscible water containing phases. These usually contain polymers (such as polyethylene glycol or PEG) and concentrated inorganic salt solutions and are shaded in light grey (Table 1). More recently, an ionic liquid / concentrated inorganic salt solvent system (medium grey in Table 1) has been tested in LLC, and has higher solute capacities than PEG solvent systems.[20-22]

Table 1 A comparison of four aqueous biphasic solvent systems[7,23-26]

Aqueous biphasic solvent system	Stationary Phase Composition (mol%)	Mobile Phase
Water – Hexane – [C_{12}mim][DiIOP] (Fig. 1)	**Water 75%, Hexane 23.5%, [C_{12}mim][DiIOP] 1.5%**	**Water**
Water-PEG-$K_2[HPO_4]$	Water-polyethylene glycol	Water - $K_2[HPO_4]$
[C_4mim]Cl-2.5M $K_2[HPO_4]$-Water	87% water, 13% [C_4mim]Cl	Water – 4M $K_2[HPO_4]$
Water - PEG - Dextran	Water - Dextran	Water - PEG

PEG = polyethylene glycol, [C_4mim]Cl = 1-butyl-3-methylimidazolium chloride, [C_{12}mim][DiIOP] = 1-dodecyl-3-methylimidazolium diisooctylphosphinate (or di(2,4,4-trimethylpentyl)phosphinate).

Experimental

Phase retention Curves

A biphasic solvent system was made by mixing water (2000 ml), ethyl ethanoate (1000 ml). To mixture 950 ml of water saturated ethyl ethanoate phase and 1000ml water saturated with ethyl ethanoate phase (MP) in a 3000 ml beaker, 1-decyl-3-methylimidazolium di-(2,4,4-trimethylpentyl)-phosphinate [C_{10}mim] [DiIOP] (50.0 g) was added to make an approximately 5% solution of [C_{10}mim] [DiIOP] dissolved in 950 ml of ethyl ethanoate. The NMR spectra of this solvent system (upper stationary phase (SP) and lower mobile phase (MP) was recorded to determine the composition of this biphasic mixture. The AECS/ECOM CPC instrument (Figures 3 and 4) was washed out with ethanol and all pumps and the instrument were filled with mobile phase, to displace the ethanol. The solvent reservoir was filled with 1 litre of MP and 1 litre of SP, and the Pump 2 was filled with SP from the top of the solvent reservoir. The instrument was filled with stationary phase through Pump 2, and the displaced mobile phase was returned to the solvent reservoir *via* the return pipe (Spider valve position = B1, VICI flow direction valve set to Position B to make the least dense phase become the stationary phase) with the rotation rate set to 400 RPM. When the instrument was full of SP, Pump 2 was stopped. The stationary phase retention curve for 5 wt% [C_{10}mim][DiIOP] + ethyl ethanoate / water solvent system was performed as follows:

(a) The level of the phase boundary was recorded at start of experiment.
(b) Spider valve position set to A1, and the VICI valve was set to position B
(c) Pump 1 set to flow rates increasing in the following order 3.0, 4.0, 5.0, 7.0, 8.5, 10.0, 12, 15, 20, 25, 30, 35, 40 ml/min.
(d) For each flow rate, take reading of the MP / SP level (the SP/MP phase boundary) in the solvent reservoir after the level in the solvent reservoir had reached a stable level, and have only mobile phase passing through the detector (no sharp peaks in the UV-Vis detector output due to stationary phase passing through the detector.
(e) For each flow rate, measure the pressure reading on the pump pressure sensor.

(f) For each flow rate, calculate the % stationary phase retention value (SPR) in the CPC rotor, using a value of 12 cm^3 for the dead volume (DV - the internal volume of the pipes, detector, valves *etc.*) and 900 cm^3 for the internal volume or capacity of the rotor (RC). % SPR = 100 x (IL-L-DV)/RC.

(g) Figures 5 and 6 shows the SPR graphs of the 5% [C_{10}mim][DiIOP] + ethyl ethanoate / water solvent system at 400 RPM and 30 C.

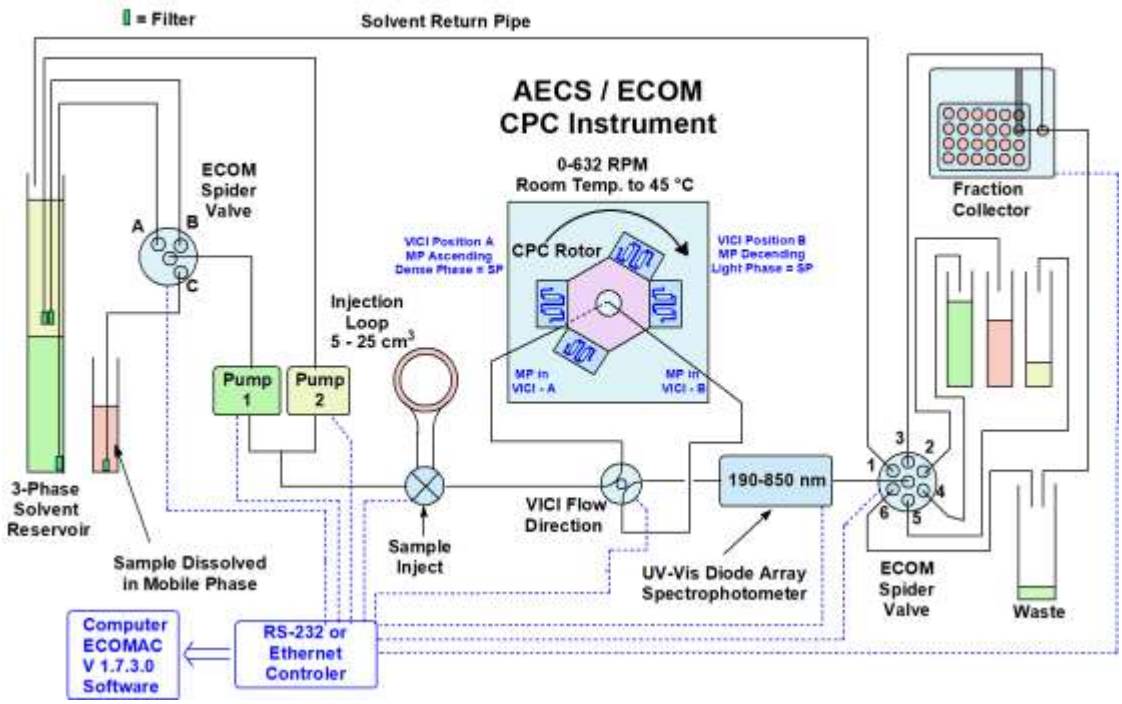

Figure 3 The full schematic of the full AECS / ECOM CPC instrument in laboratory 02.201. The instrument is set up to use biphasic solvent systems and can use UV-Vis spectrometer to control the Spider and VICI valves, and pumps allowing collection of samples with specific absorption peaks or spectra. The computer control of the detector, pumps, valves and fraction collector allows fully automated separations.

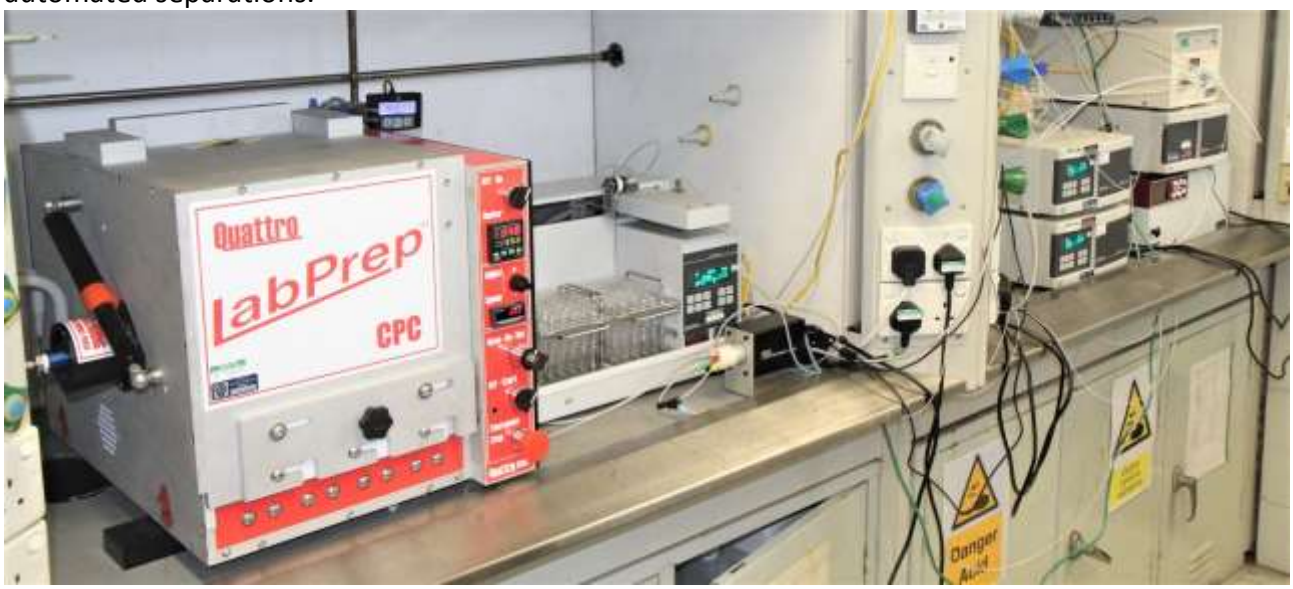

Figure 4 The AECS centrifugal partition chromatography (CPC) machine installed in the QUILL Laboratories.

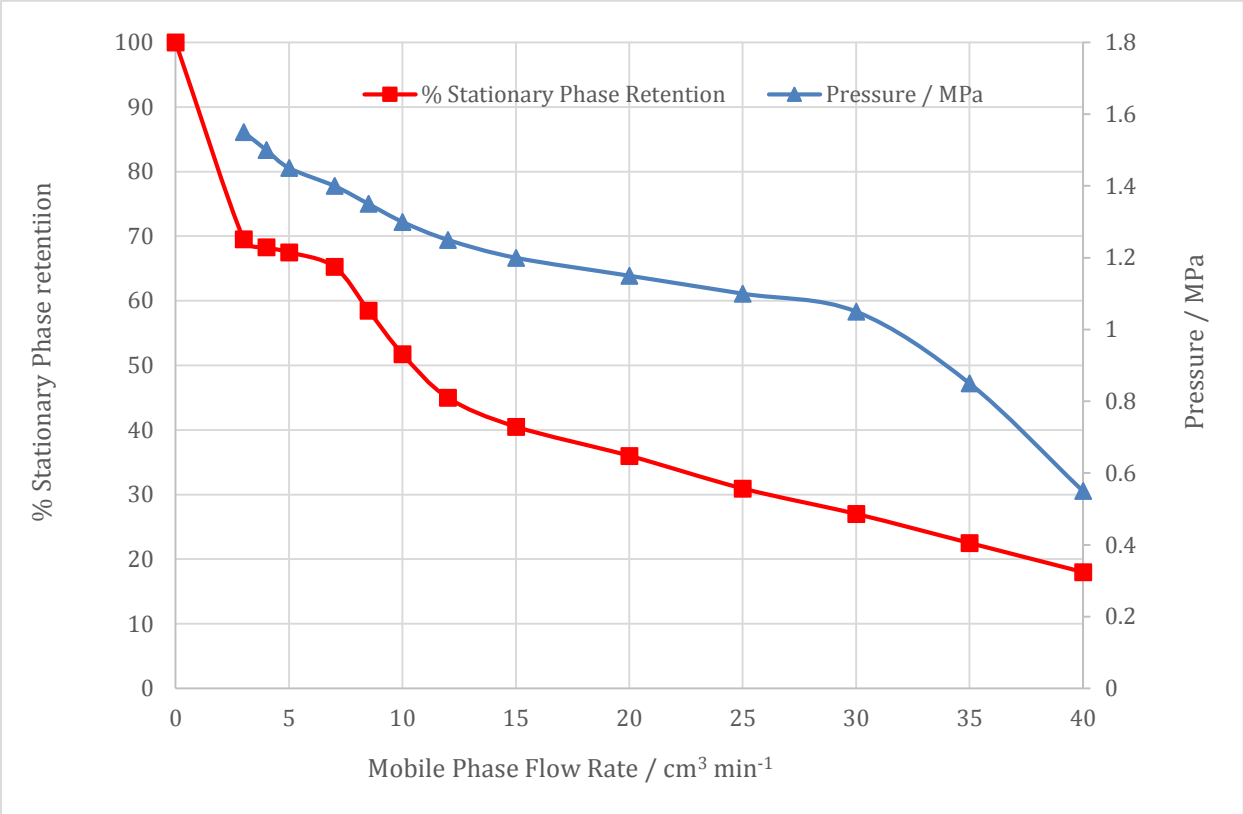

Figure 5 The % stationary phase retention curve and pressure for the water / ethyl ethanoate + 5.0 wt% [C_{10}mim][DiIOP] at 400 RPM and 30 °C, with ethyl ethanoate saturated water as the mobile phase.

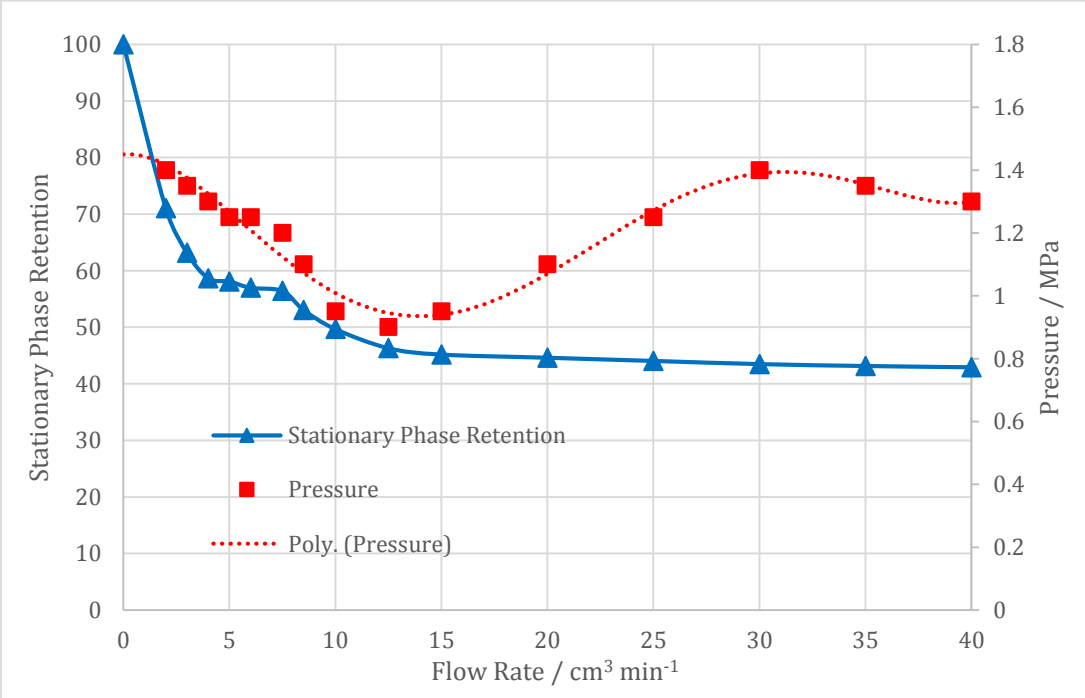

Figure 6 The % stationary phase retention and pressure *vs* the square root of the flow rate for the water / ethyl ethanoate + 10 wt% [C_{10}mim][DiIOP] at 400 RPM and 40 °C, with water as the mobile phase.

The stationary phase retention curves and corresponding CPC inlet pressure are shown in Figures 5 and 6. The deviation from ideal behaviour at 3-10 cm^3 min^{-1} flow rates is thought to be due to wetting effects of the microemulsion phase in the CPC rotor. Otherwise, the stationary phase retention (SPR) is proportional to the square root of the flow rate (Figure 6). The optimal flow rate for separations (where the gradient of the SPR curve is the lowest) with this solvent system is in the range of 3.0-7.0 cm^3 min^{-1}.

Protein separations

A model protein separation of lysozyme / cytochrome C was tested to determine whether microemulsion solvent systems can be used in separations using CPC instrument shown in Figures 6 and 7. The solvent system chosen was a water / ethyl ethanoate solvent system containing the ionic liquid [C_{10}mim][DiIOP].

The distribution ratio of lysozyme between water and ethyl ethanoate containing [C_{10}mim][DiIOP] was measured by UV-Vis spectroscopy. A biphasic solution containing water and ethyl ethanoate was prepared and 10 cm^3 of each phase of this solvent system were placed in a 40 cm^3 centrifuge tube. 25 mg of lysozyme was added and the mixture shaken until the lysozyme dissolved. The tube was places in a centrifuge and spun at 4400 RPM for 10 minutes, to allow both phases to become clear. The UV-Vis spectrum of both phases was recorded from 190-1100 nm using a 1.00 cm path length quartz UV-Vis cell. The absorption at 280 nm for lysozyme relative to the background at 350 nm was used to measure the concentration of lysozyme in each in each phase. The distribution ratio of lysozyme was then determined by dividing the absorbance of lysozyme in the stationary (ethyl ethanoate) phase by the absorption of lysozyme dissolved in the aqueous mobile phase. Increasing amounts of [C_{10}mim][DiIOP] were added to the mixture in the centrifuge tube, and the absorptions at 280 nm were determined for both phases, and the variation of distribution ratio was calculated and plotted graphically in Figure 7.

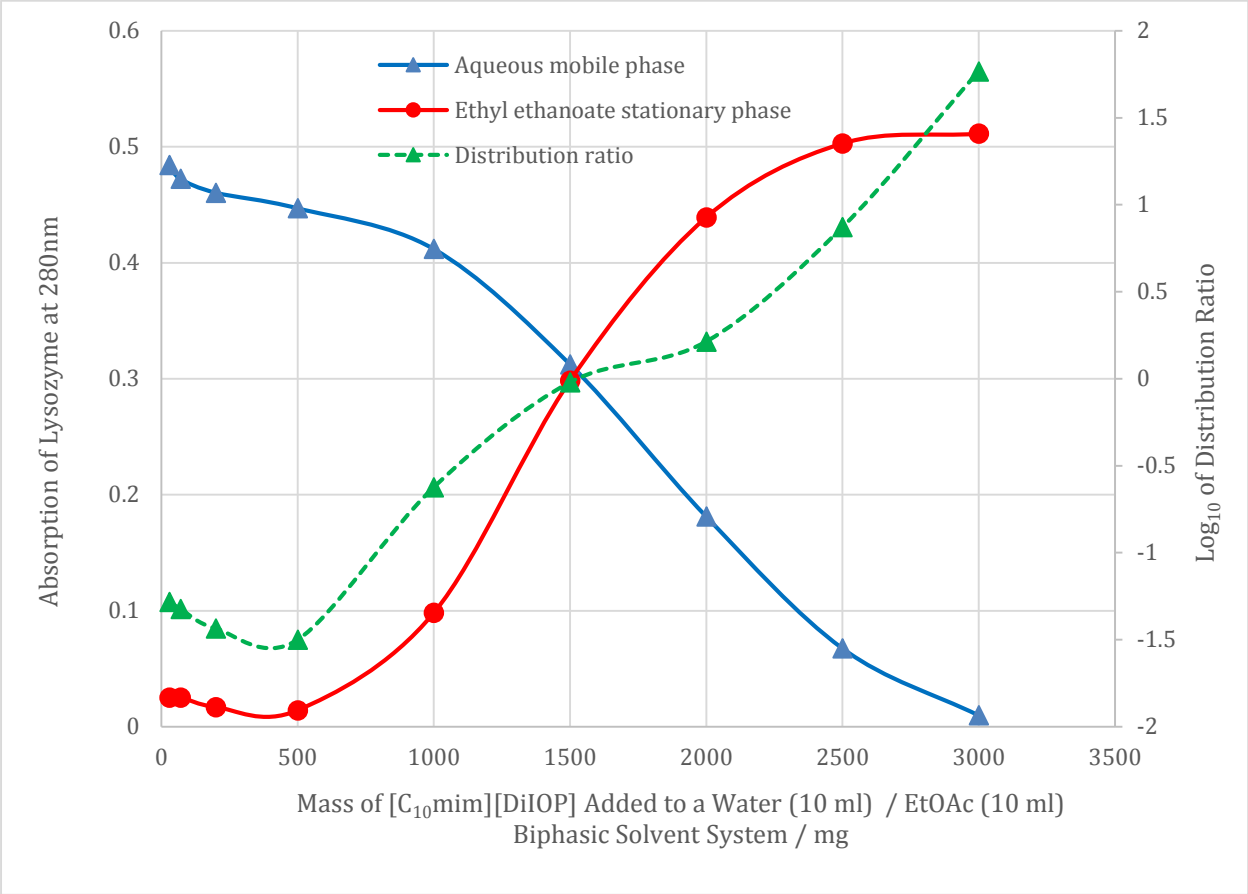

Figure 7 Variation in the absorbance of lysozyme (25 mg) dissolved in a biphasic water / ethyl ethanoate solvent system consisting of 10 cm^3 of each phase with the mass of $[C_{10}mim][DiIOP]$ added to the ethyl ethanoate phase. The absorbance values are the absorbance of lysozyme at 280 nm – the background absorbance at 350 nm. The distribution ratio was calculated by dividing the lysozyme absorbance (280 nm absorbance – 350 nm absorbance) in the stationary phase with the absorbance of lysozyme (280 nm absorbance – 350 nm absorbance) in the mobile (water) phase.

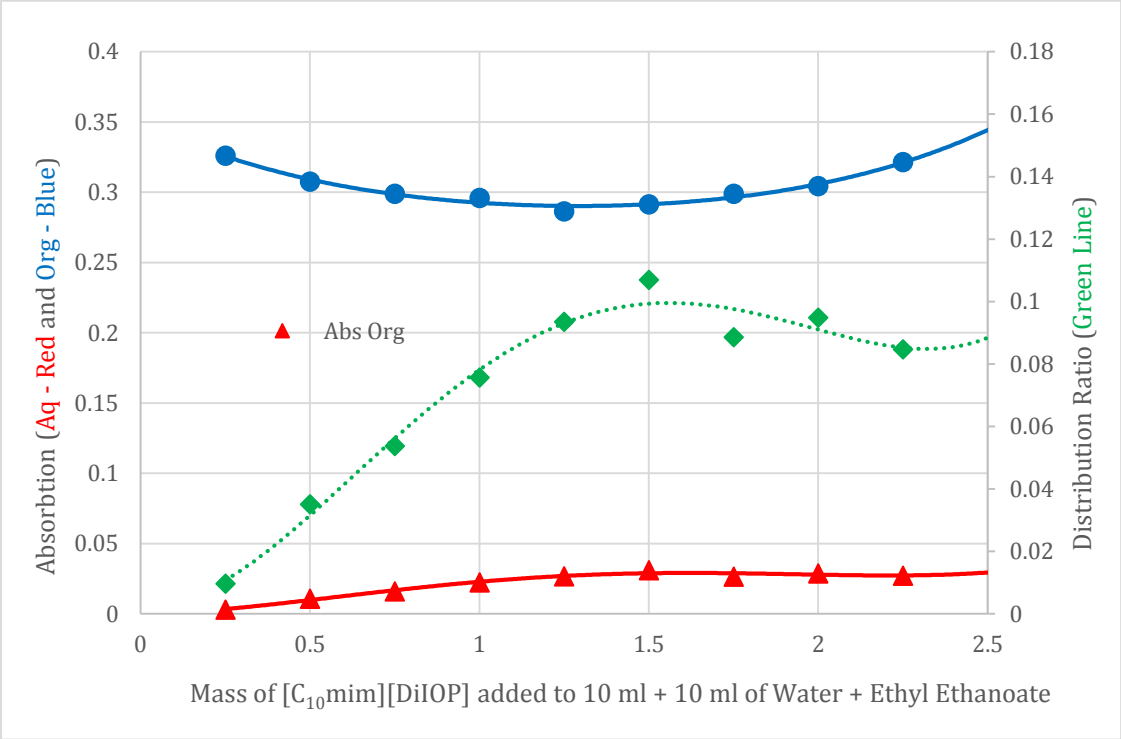

Figure 8 Variation in the absorbance of cytochrome C (2.5 mg) dissolved in a biphasic water / ethyl ethanoate solvent system consisting of 10 cm^3 of each phase with the mass of [C_{10}mim][DiIOP] added to the ethyl ethanoate phase. The absorbance values are the absorbance of cytochrome C at 410 nm – the background absorbance at 410 nm (derived from the average of the absorbance at 370 nm and the absorbance at 450 nm). The distribution ratio was calculated by dividing the cytochrome C absorbance in the stationary phase with the absorbance 410 nm in the mobile phase. The composition of the solvent system water / ethyl ethanoate + [C_{10}mim][DiIOP] was measured by adding known weights of [C_{10}mim][DiIOP] to a mixture of 10.0 cm^3 of water saturated ethyl ethanoate and 10.0 cm^3 of ethyl ethanoate saturated water in a centrifuge tube. After each addition of [C_{10}mim][DiIOP], the tube was centrifuged at 4400 RPM for 10 minutes and the ^{1}H NMR spectrum of both phases was measured in CD_3OD. The composition of the water / ethyl ethanoate + [C_{10}mim][DiIOP] solvent system is shown in Figure 9 and the mobile phase is shown in Figure 10.

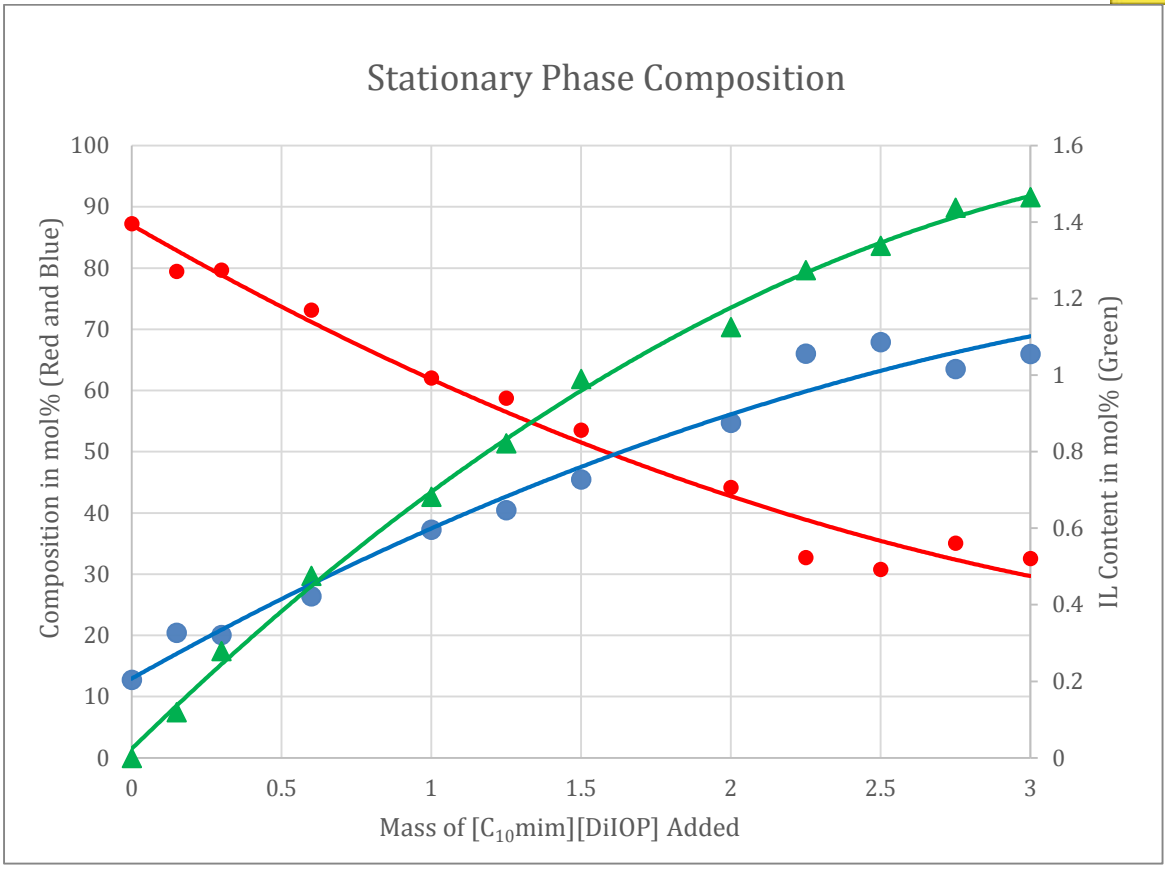

Figure 9 The composition of the stationary phase (10 cm^3 of the upper ethyl ethanoate phase) plotted against mass of $[C_{10}mim][DiIOP]$ added to the mixture of 10 cm^3 MP + 10 cm^3 SP. Water = Blue, ethyl ethanoate = red and $[C_{10}mim][DiIOP]$ = green. Error = ± 5% in % composition data points for water and ethyl ethanoate, and 0.10% mol% in ionic liquid content data points.

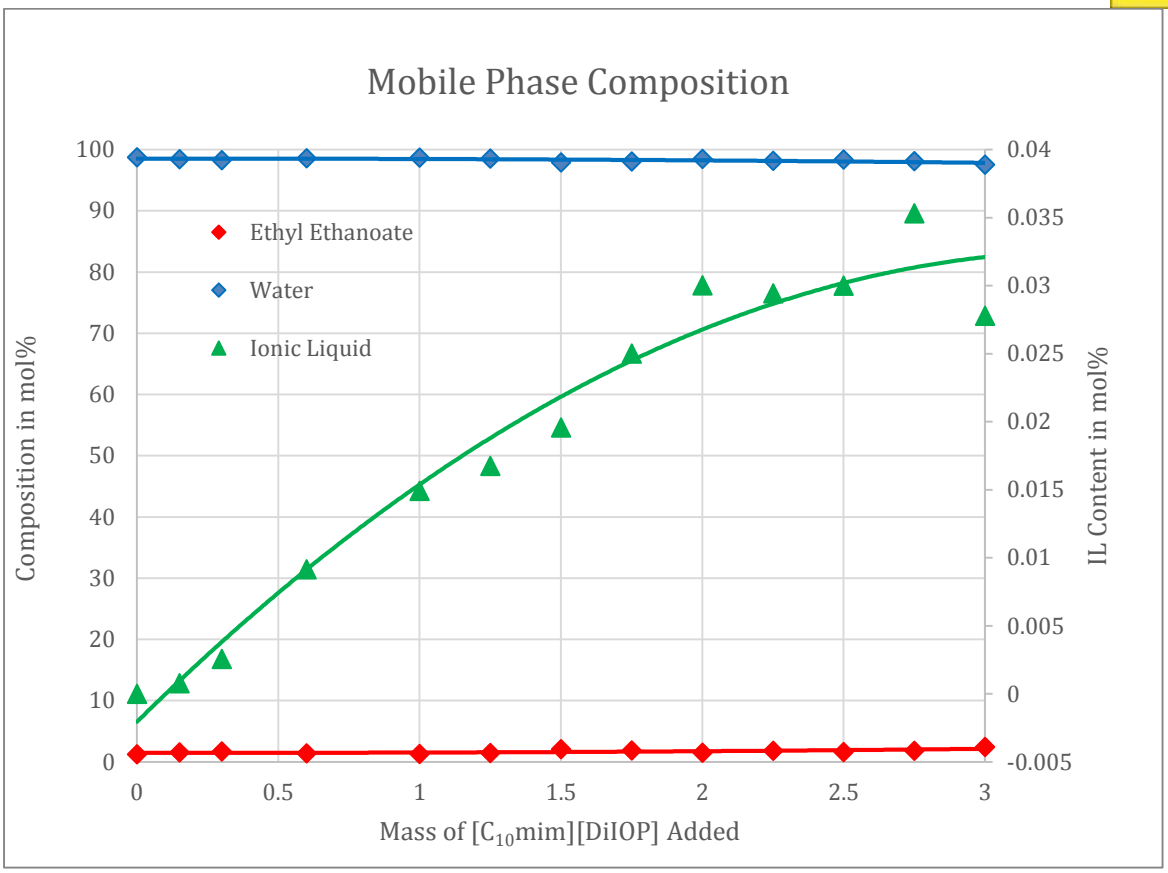

Figure 10 The composition of the mobile phase (10 cm^3 of the lower water phase) plotted against mass of [C_{10}mim][DiIOP] added to the mixture of 10 cm^3 MP + 10 cm^3 SP. Error = ± 1% in % composition data points for water and ethyl ethanoate, and 0.006 mol% in ionic liquid content data points.

The graph (Figure 9) shows that the ionic liquid [C_{10}mim][DiIOP] causes water to dissolve in the hydrophobic ethyl ethanoate phase, and generates an aqueous biphasic solvent system, the composition of which, and the water content of the stationary phase can be controlled by the amount of ionic liquid added. In Figure 10, the aqueous MP composition remains relatively stable, remaining at 1.5 to 2.5 mol % ethyl ethanoate and 98.5-97.5 mol% water, as the amount of ionic liquid [C_{10}mim][DiIOP] is increased in the solvent system. From these data, the distribution ratio of the ionic liquid (Figure 11) remains at 40-50.

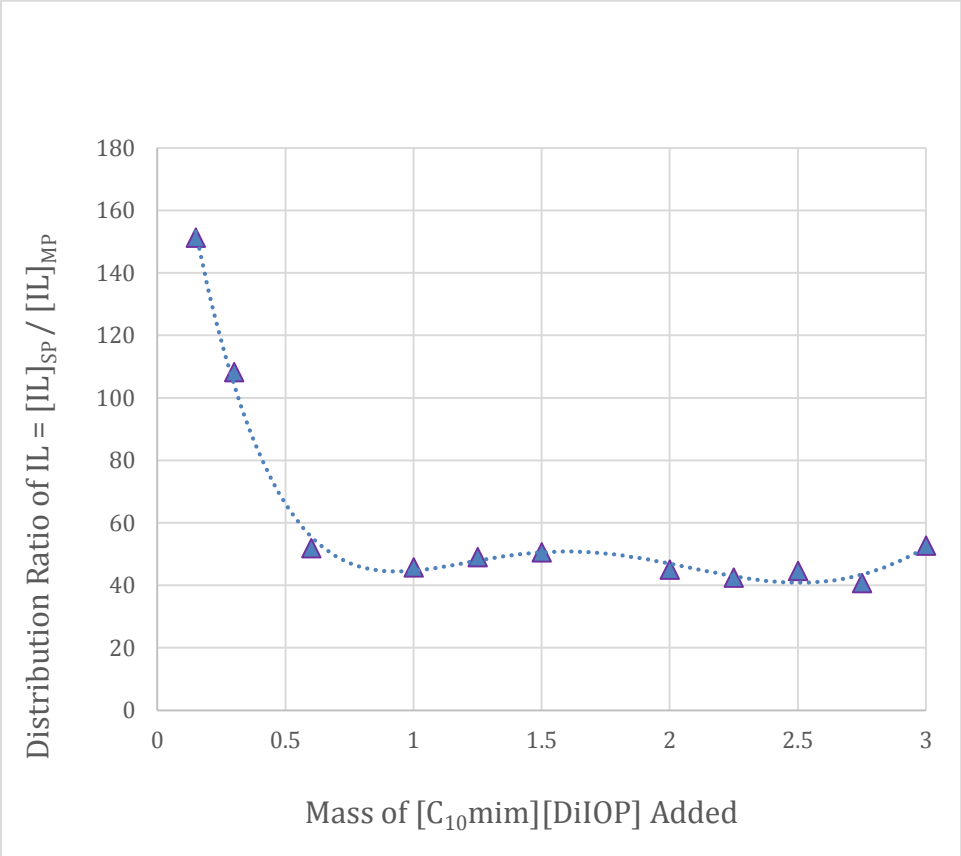

Figure 11 The distribution ratio of the ionic liquid [C10mim][DiIOP] between the SP and MP plotted against mass of [C_{10}mim][DiIOP] added to the mixture of 10 cm^3 MP + 10 cm^3 SP.

It is now possible to generate aqueous biphasic solvent systems which have a highly variable water content in the water immiscible stationary phase. As a result, solvent systems can be designed to suit a particular protein separation process. An example of how the distribution ratio can be controlled in this way is shown in Figure 12.

Figure 12 Four examples of how Cytochrome C distributes itself between water (lower phase) and ethyl ethanoate + [C_{10}mim][DiIOP] in the upper phase. The amount of [C_{10}mim][DiIOP] increases from left to right and cytochrome C goes from being completely water soluble to soluble in the upper microemulsion stationary phase.

Separation Procedure

A biphasic mixture of water (2000 cm^3) and ethyl ethanoate (1200 cm^3) was prepared and the layers were separated. 2000 cm^3 of the aqueous phase and 950 cm^3 of the ethyl ethanoate phase were combined and 50g [C_{10}mim][DilOP] was added, to form the water / 5 wt% [C_{10}mim][DilOP] + ethyl ethanoate solvent system. The 10 wt% [C_{10}mim][DilOP] solvent system was prepared from 2000 cm^3 of the above water phase, 900 cm^3 of ethyl ethanoate phase and 100g of [C_{10}mim][DilOP]. The CPC machine was filled with the stationary phase (ethyl ethanoate + 5 wt% or 10 wt% [C_{10}mim][DilOP]). The rotation rate was set to 400 RPM (5% phase) or 450 RPM (10% phase) at 30 °C (5% phase) or 40 °C (10% phase). The mobile phase (water saturated with ethyl ethanoate) was pumped into the CPC machine at 8.0 cm^3 min^{-1} (spider valve = position A1 and VICI valve = position B). For 4 hours until the reading on the detector had stabilised. A solution of 0.50 g lysozyme and 0.020 g cytochrome C was in 40 cm^3 of mobile phase was prepared and loaded into the container for Spider valve position C. The MP flow rate was reduced to 5.0 cm^3 min^{-1} and 20 cm^3 of sample was loaded into the CPC machine (spider valve = position C1, for 4.0 minutes), then the spider valve was set to position A1 for 100 minutes. The separated cytochrome C fraction was collected from 100-130 minutes (spider valve = position A4), and the lysozyme was collected from 130-200 minutes (spider valve = position A2). The separation was stopper after 250 minutes. The chromatogram is shown in Figure 13.

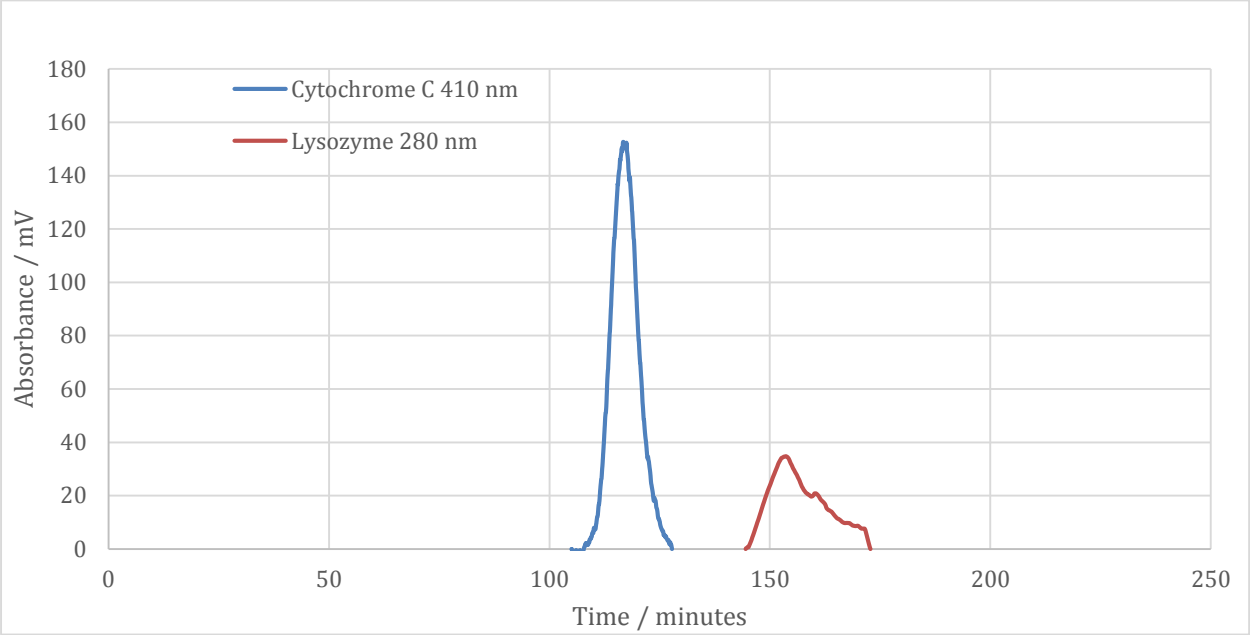

Figure 13 The chromatogram of 0.0125 g of Cytochrome C (410 nm) and 0.20 g of lysozyme (280 nm) using a 10.0 wt% [C_{10}mim][DilOP] dissolved in water saturated ethyl ethanoate (900 cm^3, stationary phase) and of ethyl ethanoate saturated water (2000 cm^3, mobile phase) solvent system. The chromatogram was run 5 cm^3 min^{-1} at 450 RPM and 40 °C with cytochrome C measured at 410 nm and lysozyme measured at 280nm, with a baseline recorded at 350 nm. The CPC rotor was underfilled with stationary phase at 7 cm^3 min^{-1}.

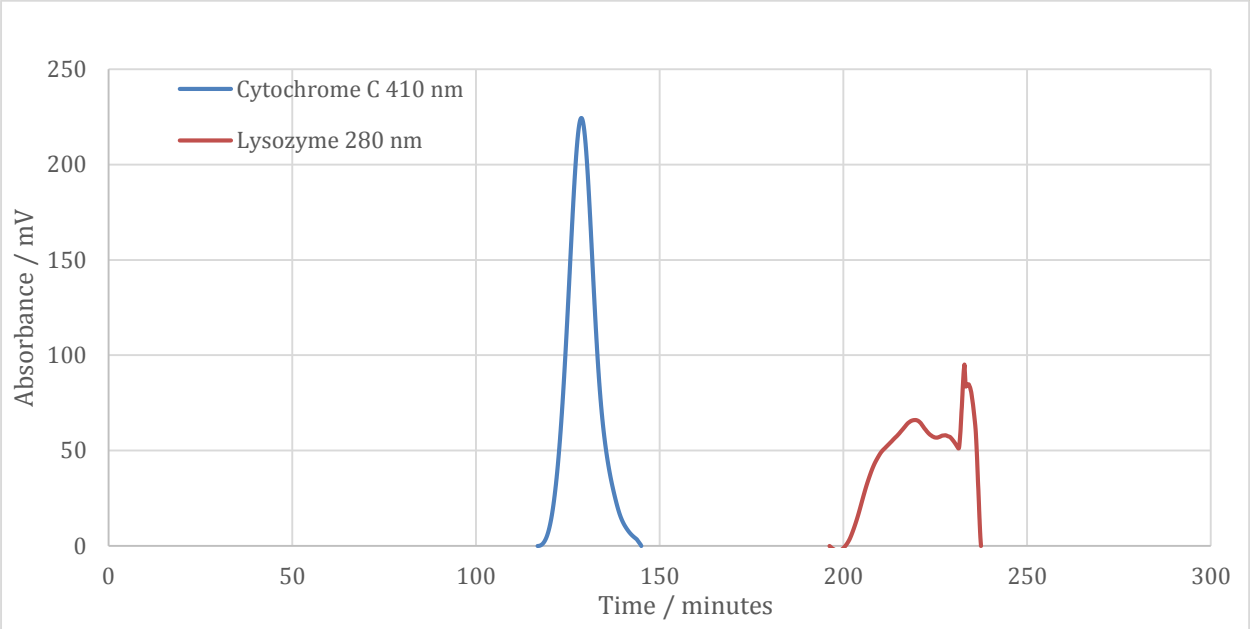

Figure 14 The chromatogram of 0.020 g of Cytochrome C (410 nm) and 0.25 g of lysozyme (280 nm) using a 10.0 wt% [C_{10}mim][DiIOP] dissolved in water saturated ethyl ethanoate (900 cm^3, stationary phase) and of ethyl ethanoate saturated water (2000 cm^3, mobile phase) solvent system. The chromatogram was run at 7 cm^3 min^{-1}, at 450 RPM and 40 °C with cytochrome C measured at 410 nm and lysozyme measured at 280nm, with a baseline recorded at 460 nm. The CPC rotor was underfilled with stationary phase at 7 cm^3 min^{-1}.

Two separations were performed using the 5 wt% and 10 wt% [C_{10}mim][DiIOP] containing mixtures of water and ethyl ethanoate, with water as the mobile phase and ethyl ethanoate / [C_{10}mim][DiIOP] as the stationary phase. For the 5% [C_{10}mim][DiIOP] solvent system, only a complete separation was obtained for both the 5% and 10% [C_{10}mim][DiIOP] solvent systems. The separations are shown in Figures 13 and 14. This provides a proof of concept that protein separations are feasible using water / microemulsion solvent systems.

Composition of 5pc [C_{10}mim][DiIOP] solvent system by NMR.

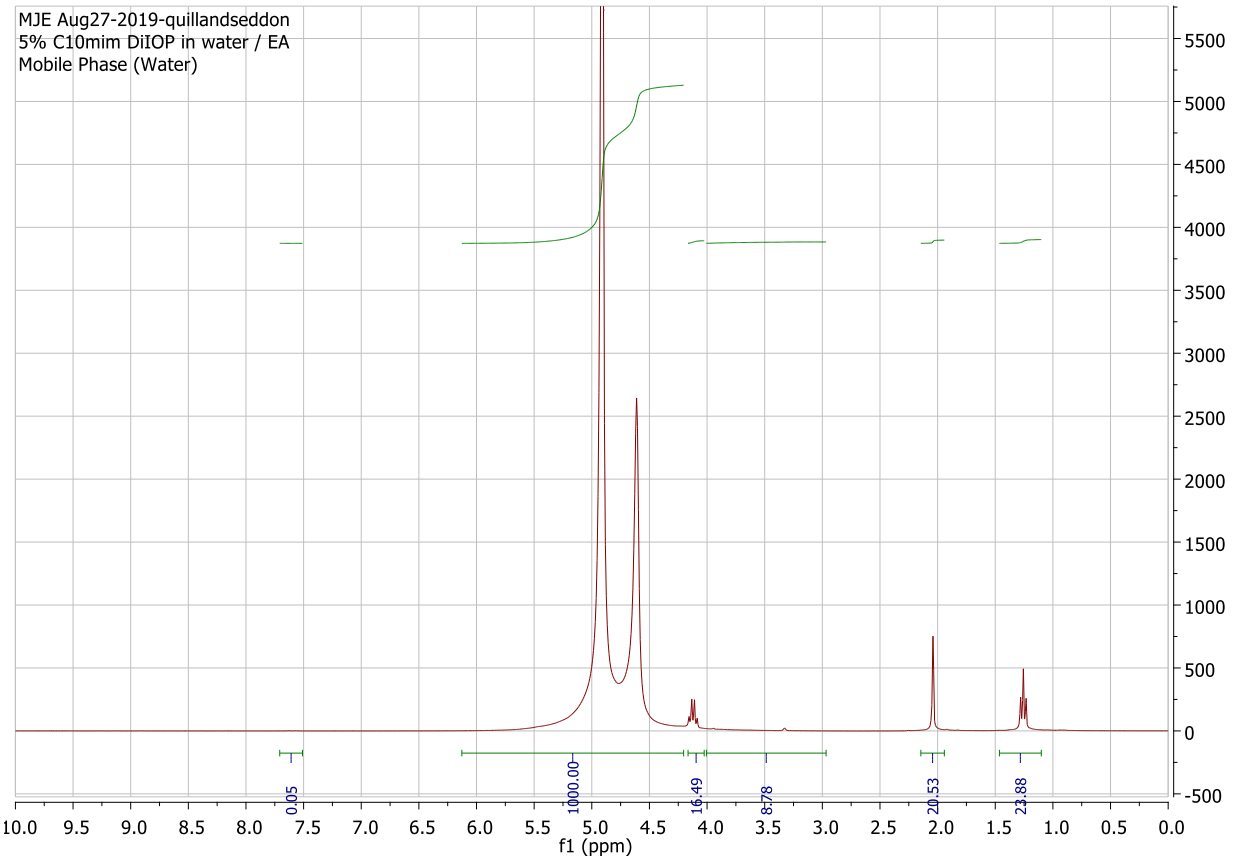

Figure 15 5% [C_{10}mim][DiIOP] in water / ethyl ethanoate: mobile phase. Water = 98.47 mol%, EA = 1.521 mol% and IL = 0.0059 mol%.

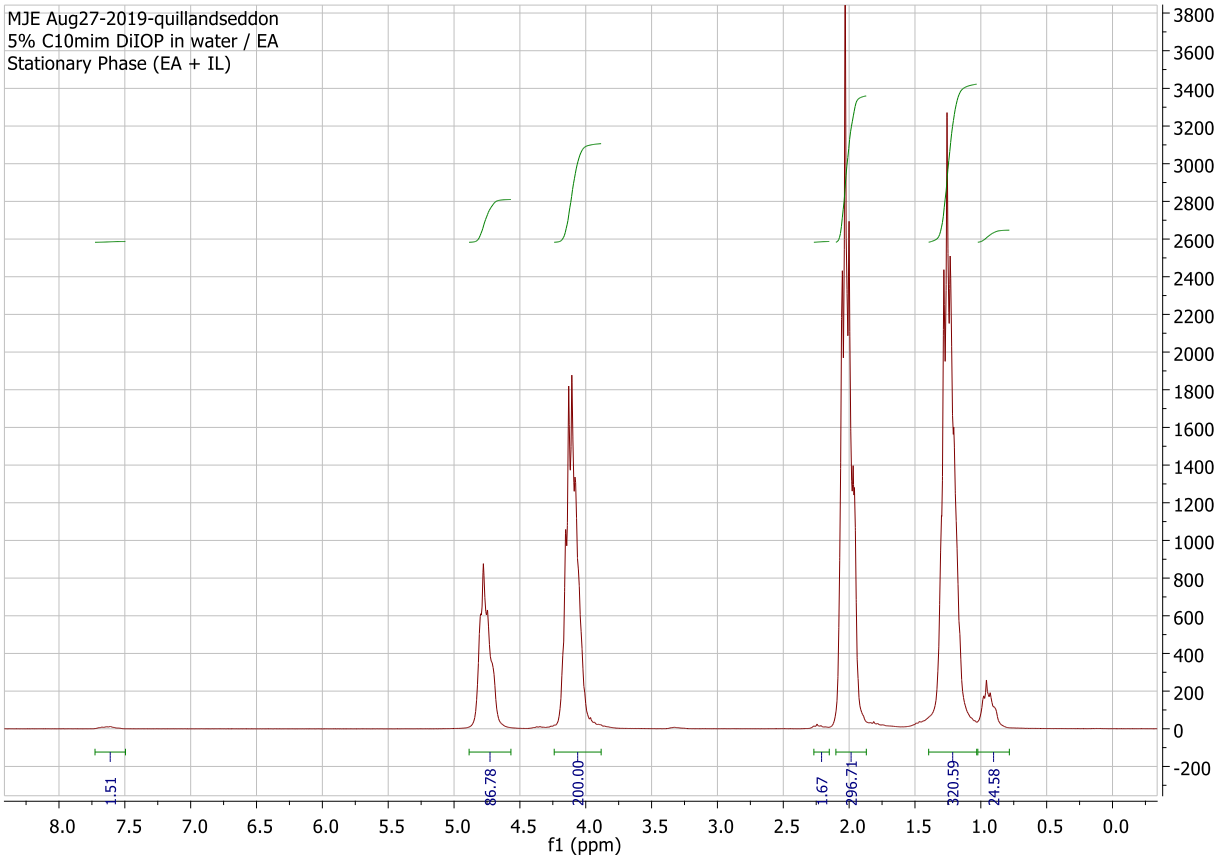

Figure 16 5% [C_{10}mim][DiIOP] in water / ethyl ethanoate: stationary phase. Water = 30.10 mol%, EA = 69.37 mol% and IL = 0.53 mol%.

Composition of 5pc [C_{10}mim][DiIOP] by NMR.

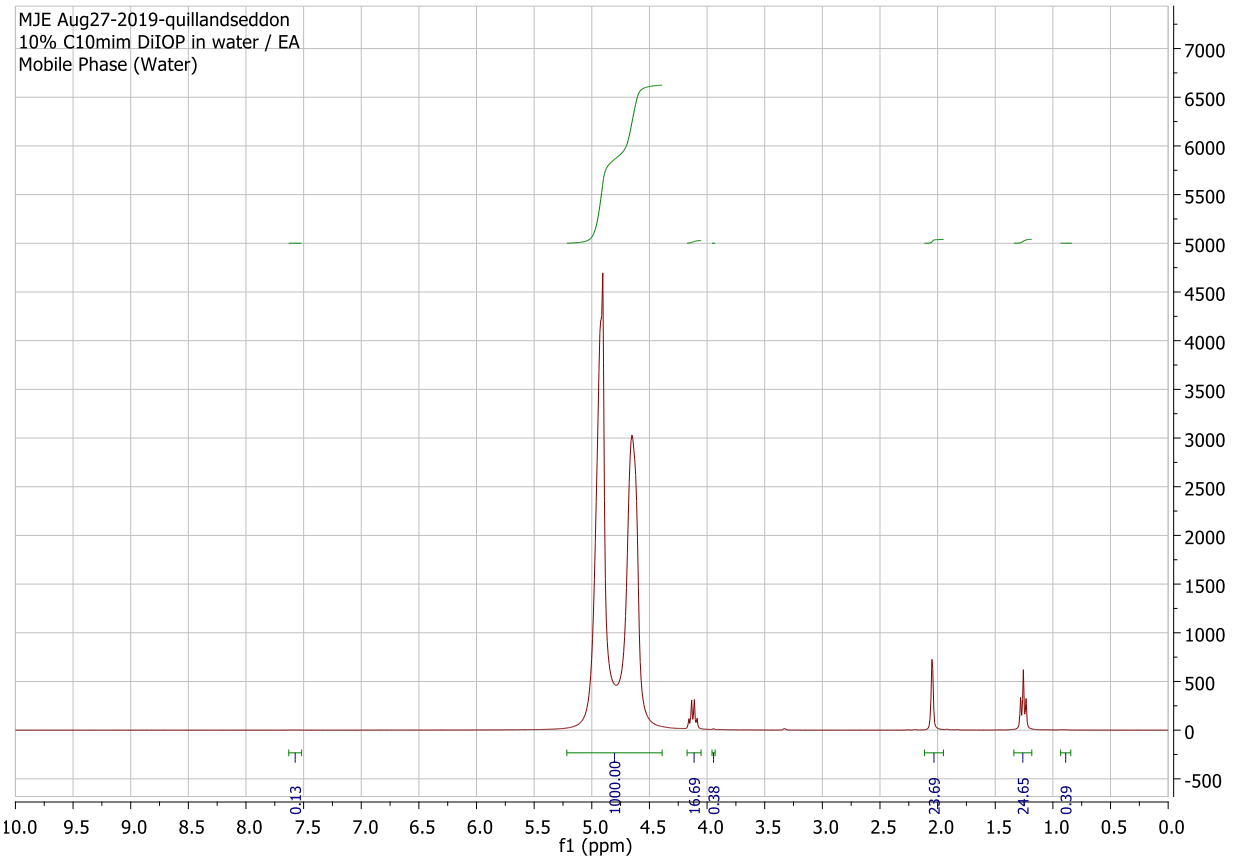

Figure 17 10% [C_{10}mim][DiIOP] in water / ethyl ethanoate: mobile phase. Water = 97.58 mol%, EA = 2.405 mol% and IL = 0.013 mol%.

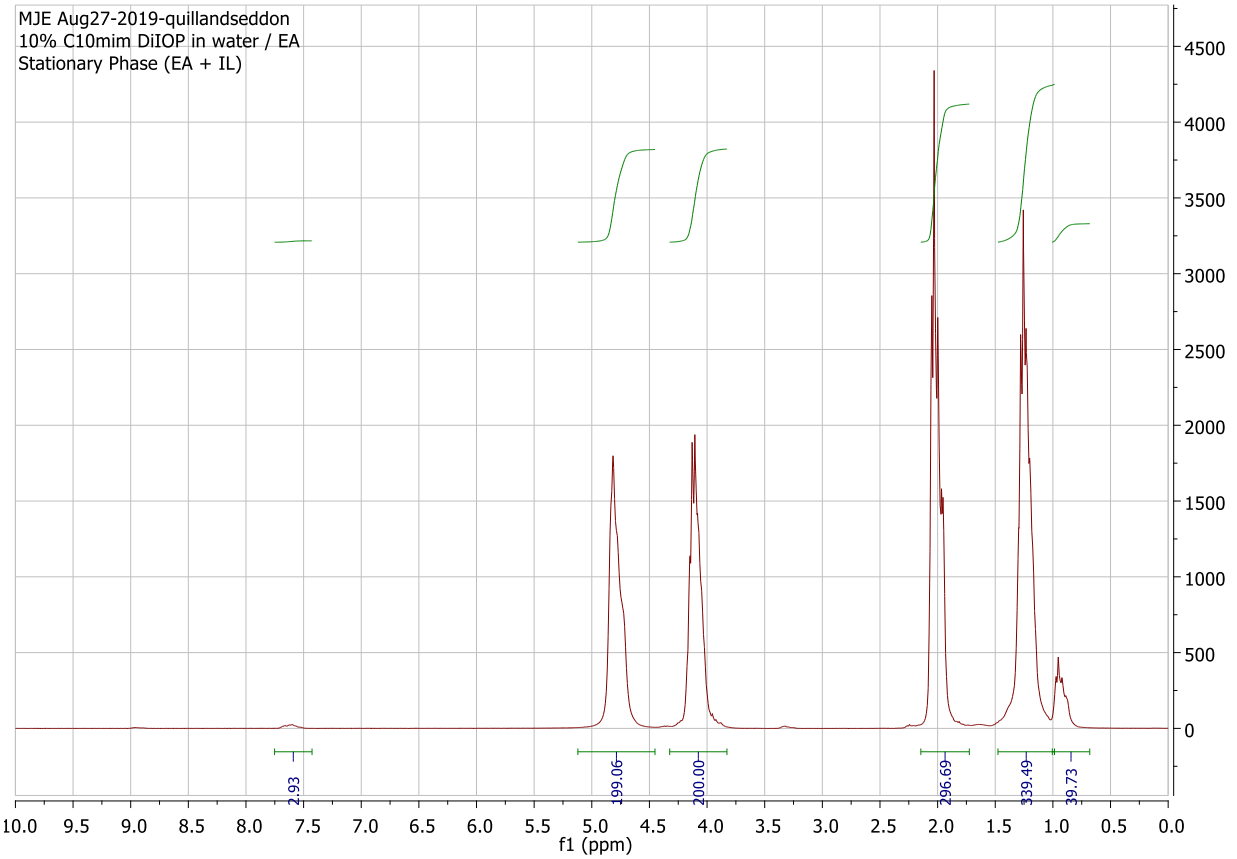

Figure 18 10 wt% [C_{10}mim][DiIOP] in water / ethyl ethanoate: stationary phase. Water = 30.10 mol%, EA = 69.37 mol% and IL = 0.73 mol%.

The composition of the two solvent systems (5wt% and 10wt% [C_{10}mim][DiIOP]) were measured by ^{1}H NMR, and are shown in Figures 15 to 18. The composition of the solvent system was close to the values in Figure 10. Since the ionic liquid has slight solubility in the mobile phase, the compositions are difficult to accurately calculate, and must be measured to give an accurate picture of the solvent system composition.

References

1. M. Freemantle, *An Introduction to Ionic Liquids*, The Royal Society of Chemistry, 2009.
2. A. Berthod and B. Billardello, *Advances in Chromatography, Vol 40*, 2000, **40**, 503-538.
3. A. Foucault and K. Nakanishi, *J. Liq. Chromatogr.*, 1990, **13**, 2421-2440.
4. H. Watarai, *J. Chromatogr. A*, 1997, **780**, 93-102.
5. M. Blesic, M. Swadzba-Kwasny, J. D. Holbrey, J. N. C. Lopes, K. R. Seddon and L. P. N. Rebelo, *Phys. Chem. Chem. Phys.*, 2009, **11**, 4260-4268.
6. I. R. Collins, M. J. Earle, S. P. Exton, N. V. Plechkova and K. R. Seddon, *World Pat.,* WO2006111712A2, 2006.
7. M. Hejazifar, M. Earle, K. R. Seddon, S. Weber, R. Zirbs and K. Bica, *J. Org. Chem.*, 2016, **81**, 12332-12339.
8. S. Y. Huang, Y. Z. Wang, Y. G. Zhou, L. Li, Q. Zeng and X. Q. Ding, *Anal. Methods*, 2013, **5**, 3395-3402.
9. L. Brown, M. J. Earle, M. A. Gîlea, N. V. Plechkova and K. R. Seddon, *Aust. J. Chem.*, 2017, **70**, 923-932.
10. C. Schroder, *Top. Curr. Chem.*, 2017, **375**, 26.
11. L. Brown, M. J. Earle, M. A. Gîlea, N. V. Plechkova and K. R. Seddon, *Top. Curr. Chem.*, 2017, **74**, 1-41.

12. G. W. Zheng, X. Y. Liu, Z. J. Zhang, P. Tian, G. Q. Lin and J. H. Xu, *RSC Adv.*, 2013, **3**, 20446-20449.13. Y. H. Guan, P. Hewitson, R. van den Heuvel, Y. Zhao, R. P. G. Siebers, Y. P. Zhuang and I. Sutherland, *J. Chromatogr. A*, 2015, **1424**, 102-110.
14. H. Rehm, *Protein Biochemistry and Proteomics*, Academic Press, Elsevier Inc., Burlington, MA 01803, USA, 2006.
15. A. Rizwan, *Protein Purification*, InTech, Rijeka, Croatia, 2012.
16. A. A. Tietze, P. Heimer, A. Stark and D. Imhof, *Molecules*, 2012, **17**, 4158-4185.
17. Y. Ito and R. Clary, *Separations*, 2016, **3**, 7.
18. K. He, Z. Y. Zou, Y. R. Hu, Y. Yang, Y. B. Xiao, P. C. Gao, X. G. Li and X. L. Ye, *J. Sep. Sci.*, 2016, **39**, 703-708.
19. K. Faure, E. Bouju, P. Suchet and A. Berthod, *Anal. Chem.*, 2013, **85**, 4644-4650.
20. M. J. Ruiz-Ángel, V. Pino, S. Carda-Broch and A. Berthod, *J. Chromatogr. A*, 2007, **1151**, 65-73.
21. Z. G. Jiang, Q. Z. Du and L. Y. Sheng, *Chin. J. Anal. Chem.*, 2009, **37**, 412-416.
22. M. J. Earle and M. A. Gilea, *World Pat.,* WO2013140185A1, 2013.
23. I. R. Collins, M. J. Earle, S. P. Exton, N. V. Plechkova and K. R. Seddon, WO 2006111712 A2, 2006.
24. M. G. Freire, A. F. M. Claudio, J. M. M. Araujo, J. A. P. Coutinho, I. M. Marrucho, J. N. C. Lopes and L. P. N. Rebelo, *Chem. Soc. Rev.*, 2012, **41**, 4966-4995.
25. R. D. Rogers, A. H. Bond, C. B. Bauer, Y. Song, J. H. Zhang and R. R. Chomko, *Abstr. Pap. Am. Chem. Soc.*, 1994, **208**, 17-IEC.
26. M. L. Moody, H. D. Willauer, S. T. Griffin, J. G. Huddleston and R. D. Rogers, *Ind. Eng. Chem. Res.*, 2005, **44**, 3749-3760.
27. V. Singh, S. Panda, H. Kaur, P. K. Banipal, R. L. Gardas and T. S. Banipal, *Fluid Phase Equilib.*, 2016, **421**, 24-32.
28. J. M. Padro, A. Ponzinibbio, L. B. A. Mesa and M. Reta, *Anal. Bioanal. Chem.*, 2011, **399**, 2807-2820.
29. H. Miyafuji, *J. Wood Sci.*, 2015, **61**, 343-350.
30. S. Hina, Y. M. Zhang and H. P. Wang, *Rev. Adv. Mater. Sci.*, 2015, **40**, 215-226.
31. H. Garcia, R. Ferreira, M. Petkovic, J. L. Ferguson, M. C. Leitao, H. Q. N. Gunaratne, K. R. Seddon, L. P. N. Rebelo and C. S. Pereira, *Green Chem.*, 2010, **12**, 367-369.
32. M. Isik, H. Sardon and D. Mecerreyes, *Int. J. Mol. Sci.*, 2014, **15**, 11922-11940.
33. V. C. A. Orr, N. V. Plechkova, K. R. Seddon and L. Rehmann, *ACS Sustain. Chem. Eng.*, 2016, **4**, 591-600.
34. http://www.grandviewresearch.com/industry-analysis/protein-purification-isolation-market
35. K. Wilson and J. Walker, *Principles and techniques of biochemistry and molecular biology*, Cambridge University Press, Cambridge, UK, 6th edn., 2005.
36. Q. L. Luo, J. D. Andrade and K. D. Caldwell, *J. Chromatogr. A*, 1998, **816**, 97-105.
37. S. S. M. Noor, B. T. Tey, W. S. Tan, T. C. Ling, R. N. Ramanan and C. W. Ooi, *J. Liq. Chromatogr. Relat. Technol.*, 2014, **37**, 1873-1884.
38. Y. Ito, T. Mitani, N. Harada, A. Isayama, S. Tanimori, S. Takenaka, Y. Nakano, H. Inui and R. Yamaji, *Journal of Nutritional Science and Vitaminology*, 2013, **59**, 358-364.
39. D. Abd El-Hady, H. M. Albishri and R. Rengarajan, *Biomed. Chromatogr.*, 2015, **29**, 925-934.
40. D. A. El-Hady, H. M. Albishri, R. Rengarajan, S. El Deeb and H. Watzig, *Electrophoresis*, 2015, **36**, 3080-3087.
41. F. Hasan, P. Vidanapathirana, S. Das, V. E. Fernand, N. Siraj, J. N. Losso and I. M. Warner, *RSC Adv.*, 2015, **5**, 69229-69237.

QUILL Quarterly Report

August 2019 – October 2019

Name:	**Andrew Forde**		
Supervisor(s):	Dr Stephen Glover, Dr Rob Watson and Prof Peter Nockemann		
Position:	PhD student		
Start date:	03/06/2019	Anticipated end date:	
Funding body:	EPSRC & Horiba-MIRA		

Battery Thermal Management and Algorithmic 3D Temperature Prediction

Background

Development of lithium-ion batteries is rapidly accelerating as consumers continue to use more battery powered devices. This includes the development of electric vehicles (EVs) which use high capacity lithium-ion batteries as an alternative fuel source to combustion of fossil fuels. Although this change provides many benefits, the performance and safety of EV batteries is a high priority in research as these are the areas holding back mass uptake by the public. Both performance and safety of the battery are addressed by managing the temperature of battery cells when in use through an on-board battery management system. This system measures the temperature of the cell and adjusts cooling and performance limits in order to keep the temperature in a safe operational range (15 °C – 30 °C). Currently, cell temperature is commonly measured by observing the temperature of casing on the cell or battery pack, both of which do not give an accurate representation of the internal temperature at which the electrochemical reactions are taking place. Therefore, a more accurate method of estimating battery internal temperature is required which will not affect the performance of the cell. If this can be predicted using external casing temperatures, this method could be introduced as part of the battery management system and therefore not require any adjustment to the vehicle instrumentation.

Objective of this work

The goal of this work is to instrument a prismatic battery cell with internal temperature sensors to allow for accurate measurement of internal temperatures across various conditions. Results of this experiment can then be used to develop a 3D predictive algorithm which allows a battery management system to accurately predict internal temperatures of the cell. The algorithm will then be implemented in a battery management system developed by Horiba and tested in a consumer EV under real-world conditions in a controlled environment.

Progress to date

- Three-month placement at sponsor company Horiba-MIRA.
    - Entropic heating project found that long relaxation open circuit voltage values can be estimated using an equivalent circuit model and a short (30 minute) voltage relaxation.
- Literature review.
- Equivalent circuit model developed using Simulink.

- Basic thermal diffusion model developed using inputs from equivalent circuit model.

Conclusions and future work

Internal resistance changes by up to 6% across the volume of the cell. Therefore, for accurate heat generation it is not suitable to assume R_{int} is homogeneous across the electrodes.

Next steps for algorithm development:

- SOC estimator using Coulomb counting.
- Parameters varying with SOC (Entropic coefficient, R_{int}, etc).
- Battery cooling effects.
- More accurate cell geometry.
- Parallel programming.

QUILL Quarterly Report

August 2019 – October 2019

Name:	**Oisin Hamill**		
Supervisor(s):	Dr Nancy Artioli (Primary) and Prof Alex Goguet (Secondary)		
Position:	PhD Student		
Start date:	01/10/2019	Anticipated end date:	30/09/2022
Funding body:	EPSRC		

Mechanism Understanding of NOx storage, Release and Reduction on Pt/Doped Ceria Catalysts

Background

Due to the strengthening of emission legislation both in Europe and North America, there is a need for further optimisation of existing emission after-treatment catalytic converters for automotive applications. High surface area ceria is successfully employed as excellent support of metals (Pd, Ru, Pt, etc.) in commercial catalytic systems for the oxidations of CO and propane and automotive emission control.

Ceria is a unique material with a rich and complex chemistry which shows marked structure sensitive properties than can be assessed through shape-controlled synthesis. It possesses the high oxygen storage capacity (OSC), a unique redox property by the cycle of Ce4+/Ce3+ redox pairs and it can increase the migration of lattice oxygen. The catalytic activity of ceria can be further enhanced using dopants.

Among all, Pt doped ceria catalysts show an enhanced NOx storage at low temperature, together with an improved CO/HC light off. It is not clear whether this is due to the presence of higher number of active sites (dopants create a more favourable environment for NOx storage), same number of sites but intrinsically more active, or enhanced NO oxidation activity (rate determining step).

It has been proposed that the dopants increase the concentration of surface vacancies which affect the ionic conductivity, oxygen mobility and oxygen storage capacity of the CeO2. It can be speculated that all these properties are responsible for the enhanced oxidation activity (CO, HC, NO) by promoting oxygen diffusion and the formation of more “reactive oxygen” species. Moreover, the oxygen vacancies could play a role in the mechanism of the reaction, favouring the NOx storage.

It has also been found that the purge efficiency of doped systems is lower compared to the un-doped catalyst. This is related to the different surface intermediates species observed during preliminary NOx storage IR experiments. However, it is unknown how this relates to the presence of dopants (modification of the rate of the redox reaction, different electronic environment which allows stronger NOx adsorption). Additionally, presence of dopants modifies

the Pt reducibility and Pt – CeO2 interaction, allowing more readily activation during rich purge and increased stability to lean deactivation. This is related to:

- Improved reducibility after a rich activation treatment
- Pt is not fully re-oxidised after the lean treatment and can be easily re-activated when exposed to the reductant present in the gas feed again.

Further characterisation is necessary to probe the enhanced promoting effect, especially after the reducing pre-treatment and greater stability to oxidising condition.

Objective of this work

1. Improve the understanding of Pt doped ceria NOx storage mechanism together with the mechanism of rich purge.
2. Gain more knowledge of the rich activation/lean deactivation mechanisms.
3. Determine the structure of the active sites under reaction conditions and differentiate between active species and spectators by transient methods.
4. Development of a global kinetic model.

Progress to date

Overview UKEM conference attended at Harwell. This covered an overview of work done in emission control areas through the EU.

Catalyst synthesis and project planning meetings attended at collaborating company headquarters – 15 Catalyst samples made and sent for initial characterisations to collaborating company testing facilities. The 3 various support samples were also taken for initial characterisations.

Test conditions discussed and established and testing rig enhancements underway.

Literature reading to gain deeper knowledge.

No results to discuss at current time.

Conclusions and future work

Future work forecast for the next 2-3 months:

Initial characterisations to be performed at QUB and compared, for control purposes, to the findings from company results.

Rig updated and necessary new gases and automation valves to be added to equipment currently present.

Water saturation column to be updated on current rig for more reliable saturation readings and temperature control.

Lean/rich cycling testing to begin and results analysed.

Literature review to be written.

QUILL Quarterly Report

August 2019 – October 2019

Name:	**Stephen Mc Dermott**		
Supervisor(s):	Dr Haresh Manyar and Prof Peter Nockemann		
Position:	PhD student		
Start date:	1st October 2019	Anticipated end date:	1st March 2023
Funding body:	EPRSC		

Catalytic Production of Biomass-Derived Liquid Transportation Fuel Additives

Objective of this work

Methods to reduce fatty acids/carboxylic acids such as octanoic acid to produce liquid transportation fuel additives using ionic liquids and sodium borohydride.

Progress to date

Ionic liquids such as $[P_{6,6,6,14}]$ $[N(CN)_2]$ and $[P_{6,6,6,14}]$ $[NTF_2]$ have been produced using literature and characterised using NMR ^1H, TGA and DSC. They were found to be produced correctly. Calibration curves using GC-FID have been produced to analyse the reaction at different time intervals. The calibration curves which have been produced were octanoic acid, octan-1-ol, n-octane and octanal.

The first reaction will involve $[P_{6,6,6,14}]$ $[N(CN)_2]$, sodium borohydride solution and octanoic acid. The reaction was left to stir in glass reactor at 25 Deg C for 2 Hours. After this time, the mixture products are extracted using dibutyl ether and analysed using GC-FID.

Future work

Next stage is to perform the reaction at different conditions to determine the selectivity of the reaction to the products (Alkane or Alcohol) and the conversion of the acid into the products. The conditions of the reactions to be varied are temperature of reaction mixture, stirring speed, amount of ionic liquid, amount of sodium borohydride, amount of acid, amount of solvent and solvent used.

QUILL Quarterly Report

August 2019 – October 2019

Name:	**Anne McGrogan**		
Supervisor(s):	Dr Gosia Swadzba-Kwasny		
Position:	Phd		
Start date:	01/10/2019	Anticipated end date:	31/03/2023
Funding body:	EPSRC		

Main Group Catalysis in Ionic Liquids

Background

The start of this project has been focused on the development of borenium ionic liquids. Previous work by the group investigated ionic liquids with chloride-free anions as frustrated lewis pair (FLP) components. The ionic liquid [Bcat(P_{888})[NTf_2] was investigated as an ionic liquid FLP for the activation of H_2. This ionic liquid was combined with one equivalent of P(^tBu)$_3$ and was capable of activating H_2 at room temperature, as confirmed by ^1H and ^{31}P NMR spectroscopy. This demonstrates the potential of designer ionic liquids in FLP catalysis and potentially paves the way for their application in catalytic reactions.

Objective of this work

To further the development of new ionic liquids with highly Lewis acidic borenium cations, for applications in catalysis, in particular as frustrated Lewis pairs.

Progress to date

Synthesis of four ionic liquids – Bcat[P_{888}][NTf_2], Bcat[$P_{888}O$][NTf_2], Bcat[P_{888}][NTf_2] with 1 eq. of P(^tBu)$_3$ and Bcat[$P_{888}O$][NTf_2] with 1 eq. of P(^tBu)$_3$. These ionic liquids will then be characterised by NMR, TGA and DSC.

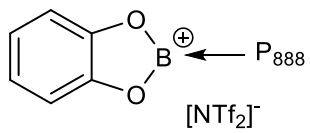

Bcat[P_{888}][NTf_2]

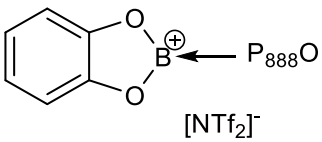

Bcat[$P_{888}O$][NTf_2]

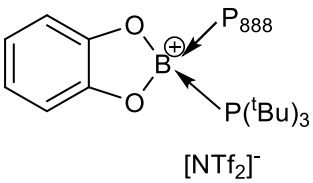

Bcat[P_{888}][NTf_2] with 1 eq. of P(^tBu)$_3$

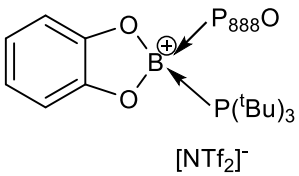

Bcat[$P_{888}O$][NTf_2] with 1 eq. of P(^tBu)$_3$

Conclusions and future work

This research will involve designing and synthesising ionic liquids displaying FLP activity, characterising them and exploring their catalytic applications. A study into the design of ionic liquids FLP systems that can activate hydrogen will be undertaken and applied to the reduction of organic substrates. Initial studies will be carried out homogenously, at NMR scale, followed by immobilisation of the IL-FLPs on solid supports and moving onto heterogenous catalysis. Activation of other small molecules, in particular CO_2 and methane, will be investigated.

QUILL Quarterly Report

August 2019 – October 2019

Name:	**Hugh O'Connor**		
Supervisor(s):	Prof Peter Nockemann and Dr Stephen Glover		
Position:	Postgraduate Research Student		
Start date:	01 October 2019	Anticipated end date:	23 March 2023
Funding body:	EPSRC		

Redox Flow Battery Materials for Energy Storage

Background

As fossil fuel supplies dwindle and the climate change problem escalates, the need to harness renewable energy resources increases. However, these energy sources are intermittent and unpredictable, making them difficult to be used in a safe and stable power grid. For this reason, it is important that new energy storage technologies are developed which can shift energy from off-peak demand times to peak demand times. One of the most promising emerging technologies is the Redox Flow battery.

In Redox Flow Batteries, Redox couples are dissolved in electrolyte solutions and stored in separate reservoir tanks. During charge and discharge these electrolytes are pumped from reservoir tanks into half cells where they react in an electrode, either consuming or generating electrons.

This working principle gives rise to a number of key advantages over other conventional battery technologies. In Flow Batteries, power and energy is decoupled; Power is controlled by the stack effectiveness whilst energy is stored in the electrolyte reservoir tanks. This makes RFBs highly customisable, allowing them to be tailored to meet the demands of various power grids. They also have a long working life; With the electrolytes stored in separate tanks, the electrodes don't undergo complex redox reactions and experience less structural changes and strain than those found in conventional batteries. One drawback of Redox Flow Batteries however is their low energy density when compared to other energy storage technologies.

Improving the energy density, energy storage efficiency and sustainability could make Redox Flow Batteries an even more promising candidate for large scale energy storage applications. This could also potentially provide a solution in reducing inevitable costs that will occur when implementing a new energy storage technology.

One method of improving the energy density of Redox Flow Batteries is designing better performing flow fields, manifolds and cell stack topologies resulting in a better performing cell stack.

Objective of this work

This project is focused on the investigation into increased performance and efficiency of redox flow batteries by improving their energy density. This will be achieved by investigating new novel flow field/ manifold designs and cell various stack topologies utilizing rapid prototyping and cost-effective manufacturing techniques.

Progress to date

To date, a thorough literature review has been carried out with a particular focus on work detailing the development and evaluation of high-performance cell designs. Furthermore, as I come from a Mechanical Engineering background and the field of Redox Flow Batteries falls at a crossroads between Chemistry and Mechanical/ Electrical Engineering, substantial time has been spent developing a better understanding of the chemistry and electrical engineering involved.

A number of promising avenues for future research have been identified such as the development of a "Radial Flow Battery" and various new flow field patterns. In recent years there has been an increasing number of researchers using Computational Fluid Dynamics (CFD) to evaluate the performance of cell designs before manufacture, similar models shall be used in future design work. Another area of particular interest is the prospect of rapid prototyping Flow Cells using 3d Printing which would allow for extra design flexibility and a wider range of experimental testing. Test prints have been designed and manufactured in the School of Mechanical and Aerospace Engineering (SMAE) and suitable materials and 3d printing technologies have been identified for use in Redox Flow Battery production.

In order to establish a baseline for the performance of cells that exist in literature, a flow cell has been designed and drawings have been produced to be manufactured using CNC machining at a future date if needed.

Other designs with novel flow field and manifolds have been drawn up using Computer Aided Design (CAS) and early CFD has been carried out to compare these designs to traditional Redox Flow Battery cells.

Conclusions and future work

In conclusion, Redox Flow Batteries with novel flow field and stack topologies appear to have great promise in developing Flow Cells with a higher Energy density. Future work will continue into the design and evaluation of these cells using a combination of CFD and experimentation of 3d Printed Flow Cells in the laboratory.

Other future work may include the design of a parametric test cell to investigate other variables that effect the performance of Redox Flow Batteries. This cell would allow "on the fly" adjustments of parameters such as electrode compression, flow field dimensions and flow pattern amongst others. Using this cell, different electrode, membrane and gasket materials and electrolyte compositions could be compared under controlled conditions. The experiments performed on this cell could help identify macro and micro design parameters that influence performance. Following on from this, in collaboration with the SMAE, machine learning could be used to identify non obvious trends and sensitivities, which could lead to an improved design with increased power density and fast transient response time.

QUILL Quarterly Report

August 2019 – October 2019

Name:	**Scott Place**		
Supervisor(s):	Dr Paul Kavanagh		
Position:	PhD Student		
Start date:	October 2019	Anticipated end date:	2022/23
Funding body:	Department for the Economy (DfE)		

Copper-Based Electrocatalysis for Energy Applications and Sensing

Background

Government funded PhD studentship focusing on electrocatalysis, with scope for energy and sensing application. We are looking at catalysts that are industrially useful and testing their potential as electrocatalysts. The project is currently very young and may be taken in one of many directions depending on where the interest of the student and supervisor lie. The work planned to be produced during this project is focused on areas that are not yet saturated and on areas where the works contributed would be useful to that body of science. This section will likely expand and mature over the coming months.

Objective of this work

To learn techniques and theory relating to electrocatalysis and general electrochemistry whilst working towards a series of publications in peer-reviewed journals before graduation with a PhD.

Progress to date

At 6 weeks into the project, we have gathered a substantial amount of data on a TEMPO-based redox polymer, PIPO, used as a catalyst for the oxidation of alcohols. The polymer has been solubility tested in a range of solvents and we have electrochemically characterised the polymer in DCM and benchmarked it against TEMPO for the oxidation of benzyl alcohol. We have also tested the stability of the catalyst using amperometry and will soon be running a similar technique, controlled-potential electrolysis, to determine the substrate conversion values over a specified amount of time for a variety of different alcohols. So far, the work has been on a proof-of-concept basis in order to bring the student up to speed with relevant techniques and theory. The student attended an International Society of Electrochemistry (ISE) student symposium at Trinity College Dublin and presented their work on PIPO as a poster.

Conclusions and future work

PIPO is a functional electrocatalyst for the oxidation of alcohols and performs competitively with the highly popular TEMPO. So far, the reactions using PIPO have been in homogenous solution. We hope to improve the performance of this catalyst by immobilising it on the electrode surface as the catalyst is currently slower due to diffusion to and from the electrode. Immobilisation would also be a proof of concept for applications in electrochemical devices such as fuel cells. In addition, we will be testing PIPO with a variety of electrode surfaces (graphite, gold, platinum) in homogenous solution to benchmark their performance. We will also be looking into the electrocatalytic performance of TEMPO-derivatives and hope to determine a rationale relating to their differences in performance.

QUILL Quarterly Report

August 2019 – October 2019

Name:	**Junzhe Quan**		
Supervisor(s):	Prof John Holbrey and Dr Leila Moura		
Position:	PhD		
Start date:	01/10/2019	Anticipated end date:	01/10/2023
Funding body:	Self funding		

Use Ionic Liquids as Draw Fluids in Water Treatment and Separation According to LCST (Lower Critical Solution Temperature) Behaviour

Background

New Ionic liquid materials have been recently developed that have lower critical solubility temperature (LCST) behaviour in water, that on heating a solution it splits into two phases. Such materials have the potential to be used as draw fluids for forward osmosis water desalination using low grade energy to address the global challenge to provide clean, accessible drinking water to all the world's populations. The program includes:

1. Preparation of ionic liquid.
2. Measurements of ionic liquid.
3. Research of using ionic liquid as draw fluid in forward osmosis.
4. Observe and measure LCST behaviour.
5. Optimise the ionic liquid to use as draw fluid.
6. Measure the energy consumption and compare with typical method of water treatment.

Objective of this work

In this research programme, new ionic liquids will be investigated as advanced fluids for forward osmosis water treatment. This offers opportunities to advance less energy intensive alternatives to conventional reverse osmosis as a solution to the global challenge of providing potable water in regions of low availability.

Progress to date

1. Experiment - Preparation of three kinds of ionic liquid, NMR to explore their structures.
2. Training - School Safety training, QUILL laboratory equipment training (Vaccum lane XRF, NMR).
3. Lecture - PGR Athena SWAN.

Conclusions and future work

Over the coming months I will measure my ionic liquid by using NMR and XRF, then I will observe the LCST behaviour by crystal16 system and finish my initial review in January 2020.

QUILL Quarterly Report

August 2019 – October 2019

Name:	**Zara Shiels**		
Supervisor(s):	Dr Artioli, Prof Nockemann and Dr Harrison		
Position:	PhD		
Start date:	Feb 2019	Anticipated end date:	2022
Funding body:	Interreg (Renewable Engine Project)		

Developing New Nanocatalysts for the Direct Conversion of Biogenic Carbon Dioxide (CO_2) to Sustainable Fuels

Background

Rising CO_2 emissions, global warming, ocean acidification and a reliance on a diminishing source of fossil fuels are all factors having a detrimental effect on the environment, making our current way of living unsustainable. In recent years, there has been a large emphasis on research that addresses these issues. Global warming is a serious problem and therefore, many governmental protocols and objectives have been put in place to tackle the issue, for example the Kyoto protocol in 1997, the Paris protocol published in 2015 and the Clean Power Plan (CPP) announced by President Obama in 2015. More recently a proposal has been signed to repeal the CPP in 2017, therefore now, more than ever, there needs to be action. One solution that has been proposed as a means of relinquishing our need for fossil fuels, is to use waste CO_2 from processes (such as anaerobic digestion) and convert this to fuels.

Typically, for gas conversion reactions to occur efficiently, a catalyst is required and in the case of CO_2 conversion to hydrocarbon fuels, iron oxide nanoparticles have exhibited high activities. Furthermore, in a drive to reduce the use of toxic solvents in chemical processes, ionic liquids can be used in the preparation of this catalyst, whilst controlling the size of the nanoparticles without the need for additional capping agents and allows for dispersion which can prevent agglomeration of the particles. Several authors have reported that by employing this synthetic method, a multi-action catalyst was obtained, with three different sites for conversion of CO_2 to hydrocarbons in the C_5-C_{11} range.

This report proposes two different possible catalyst synthesis routes that utilise these necessary ionic liquids. The first synthesis method involves the thermal decomposition of an iron precursor in a high temperature solution phase reaction. Once the reaction is complete, the produced iron (III) oxide can be separated through decantation and washed with hexane. Once fully separated, the iron (III) oxide will then be embedded within a zeolite structure for pH control and as a solid support for the final catalyst

The second novel method involves use of two iron precursors, already in the desired oxidation states, heated while stirring in the presence of a specifically chosen ionic liquid and requires less energy than previously reported syntheses. Through varying the ionic liquid utilised as the reaction solvent it is hoped we can achieve the capping capabilities of the previous reaction without the need for additional reagents.

Characterisation will be carried out at each stage of the process by a variety of methods: Nuclear Magnetic Resonance (NMR) Spectroscopy, Powder X-Ray Diffraction (PXRD), Temperature Programme Reduction (TPR), Scanning Electron Microscopy (SEM), Transmission Electron Microscopy (TEM), Brunauer-Emmett-Teller (BET) Surface Area analysis and so on.

Objective of this work

The overall aim of this project is to develop a reproducible method of synthesising a nanocatalyst for conversion of CO_2 to sustainable fuels. Synthesis and use of different ionic liquids in the preparation of the Fe_3O_4 catalyst will be carried out, as well as varying the zeolite support used, characterisation and finally high pressure testing under reaction conditions. A control will also be prepared in order to compare the novel catalyst with a conventional method.

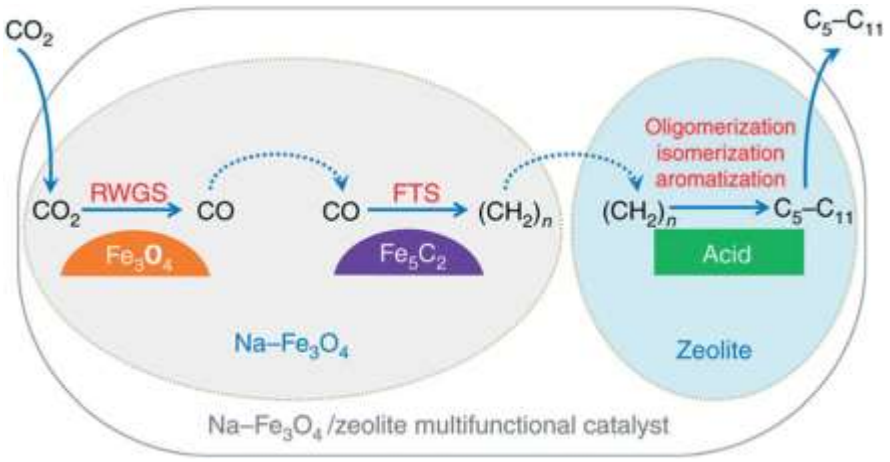

Figure 1 – Depiction of the multifunctional catalyst required for conversion of CO2 to hydrocarbons

Progress to date

The precipitation method involves first adding hydrated iron chlorides to a diluted solution of hydrochloric acid. Following this stage, dropwise addition of a precipitating agent results in the formation of a black precipitate of iron (II,III) oxide. Adequate control of the pH of the reaction mixture allows for the formed iron (II,III) oxide precipitate to remain in solution at around pH 10. Due to the magnetic nature of the produced iron (II,III) oxide nanoparticles, commonly referred to as '*Magnetite*', separation can be achieved through the use of a strong neodymium magnet.

Initially the precipitation method, as described above, was undertaken to be used as a comparison to the catalyst synthesised using both ionic liquid methods. This was successfully achieved, creating 3 different samples of high sodium, low sodium and no sodium content. These samples were then studied under XRD analysis as shown in **Figure 2**. The Scherrer equation was used to calculate the particle size for the sample with no sodium content, which was calculated to be 11.6 nm.

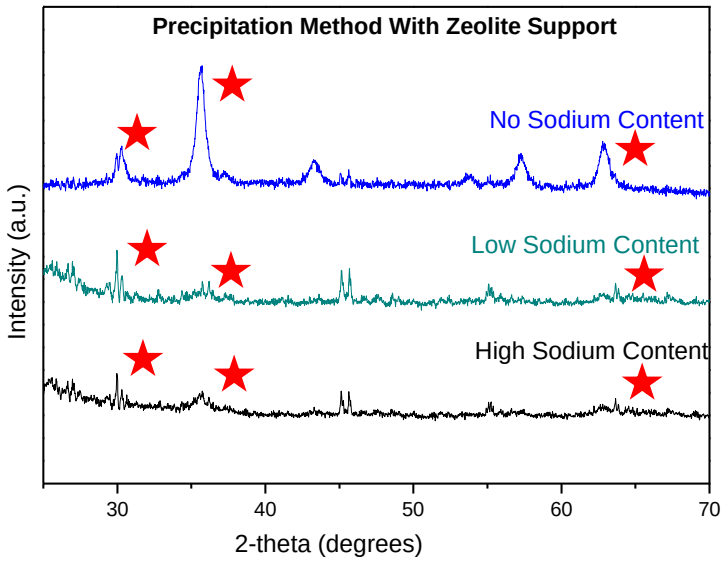

Figure 2- *XRD analysis of each precipitation method embedded on zeolite support.*

Method 1 involving 1 iron precursor was investigated. This synthesis involved 1 ml of iron precursor $Fe(CO)_5$ being added to a 100 ml round bottom flask containing 25ml of ionic-liquid $[Bmim][BF_4]$ and 1.9ml of Oleic Acid. Stabilizing agents were added in the following quantities; Oleylamine (0.3ml) and Hexadecanediol (2.7g). The reagent mixture is heated to 280°C over a period of 2 hours then kept at constant temperature for a further hour and stirred vigorously using a magnetic stirrer. The newly formed dark black solution was then washed 3 times with 25ml of Dichloromethane (DCM) and allowed to stand over a neodymium magnet for 30 mins. The black ferrous fluid is pulled out of suspension and the remaining solvent layer decanted.

The Ferrous liquid is once again washed with methanol and decanted. The wet black solid is then dried in an oil bath at 50°C under vacuum for 24 hours. Solid Iron oxide can then be extracted. The balanced symbol equation for the reaction is shown below:

$$3\,Fe(CO)_5 \xrightarrow{IL1,\ \Delta T} 3\,Fe + 5\,CO \xrightarrow[+H_2O,\ -5\,CO]{} Fe_3O_4$$

The sample was then ball milled with zeolite on a 1:1 mass ratio. The XRD analysis of this sample is shown in **Figure 3**.

Method 2, a method being developed by Queens University Belfast has also successfully produced iron oxide nanoparticles. It has been tested with and without NH_3, the later giving a yield of 70.8%. The isolation of this solid has been fully optimised with the washing of water and ethanol and repeated centrifuging and suction filtering with hopes of higher yields of both methods being established currently. Both have undergone calcination at 420°C under nitrogen in order to achieve a crystalline product. PXRD analysis of before and after calcination is shown in **Figure 3.** The Scherrer equation was used to calculate the particle sizes as summarised in Table 1.

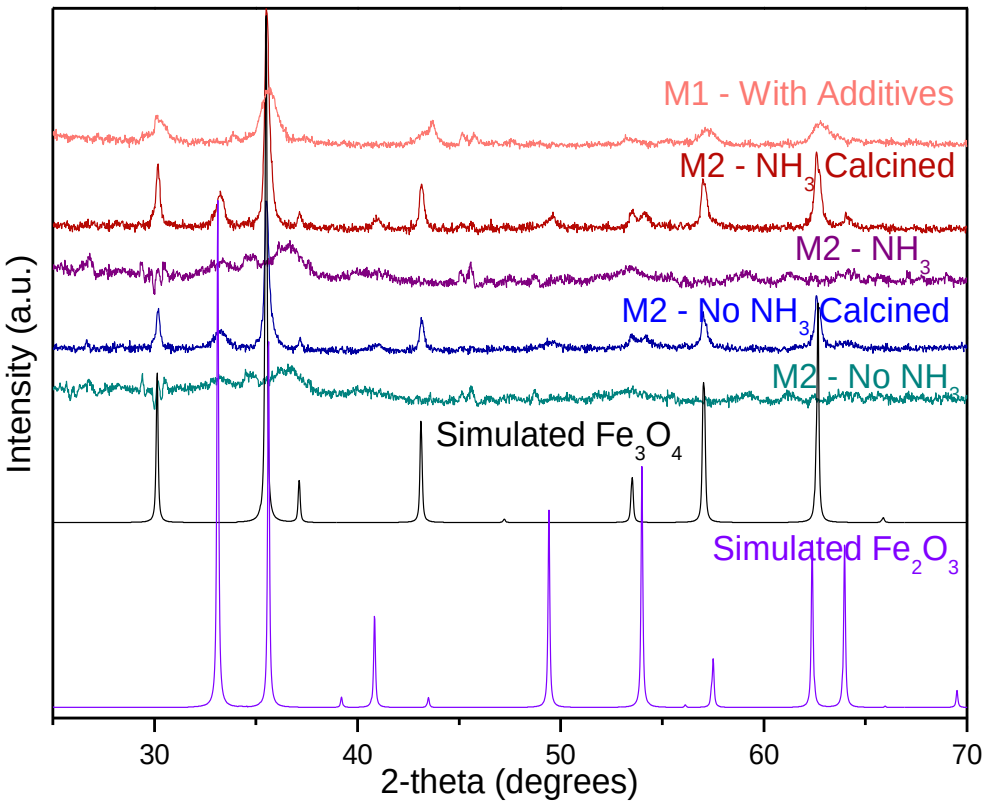

Figure 3 *- XRD analysis of methods 1 and 2 against the simulated Fe_3O_4 and Fe_2O_3 patterns.*

Method	Conditions	IL Used	Calcined	Phase Observed	Average Particle Size (nm)
1	With Additives	$[C_4mim][NTf_2]$	N	Fe_3O_4	10.5
2	With NH_3	$[C_4mim][OAc]$	N	Amorphous	13.9
2	With NH_3	$[C_4mim][OAc]$	Y	Fe_3O_4, Fe_2O_3	29.8
2	No NH_3	$[C_4mim][OAc]$	N	Amorphous	26.3
2	No NH_3	$[C_4mim][OAc]$	Y	Fe_3O_4, Fe_2O_3	40.8

***Table 1** – Summary of the iron oxide phases observed and the average particle size for methods 1 and 2.*

TEM was carried out initially on only a few samples, one sample from each method was chosen and analysed. The bright field images (BF) were acquired on a G2 Talos transmission electron microscope, operated at 200 kV.

In ionic liquid method 1, Transmission Electron Microscopy (TEM) imaging showed spherical particles that appear uniform in size and shape, with an average particle size of 10-12 nm according to interpretation of TEM imaging. These results indicate that in fact, the Fe_3O_4 particles obtained are nanoparticles and are of a suitable size for catalysis of CO_2 to hydrocarbons process. They are comparable with the TEM images reported by Wang *et al.* which featured uniform, spherical particles in a 'honeycomb' type arrangement, this group also reported an average size of 8 nm.[35]

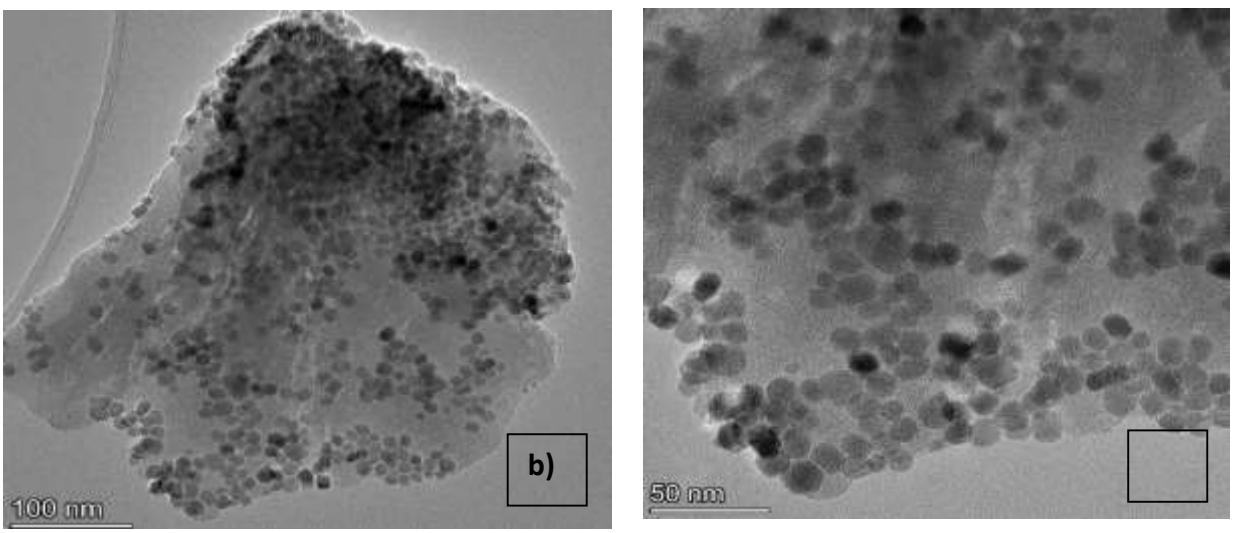

***Figure 4** - TEM Imaging of material produced by Ionic Liquid Method 1*

TEM imaging of the second ionic liquid method, where NH_3 was employed, showed elongated particles of a much more varied shape and size than those observed by Method 1. Compared to those reported by Wang *et al*. these images look much less uniform in size and shape.[35] These particles also showed a larger average particle size of 20-30 nm according to interpretation of TEM imaging.

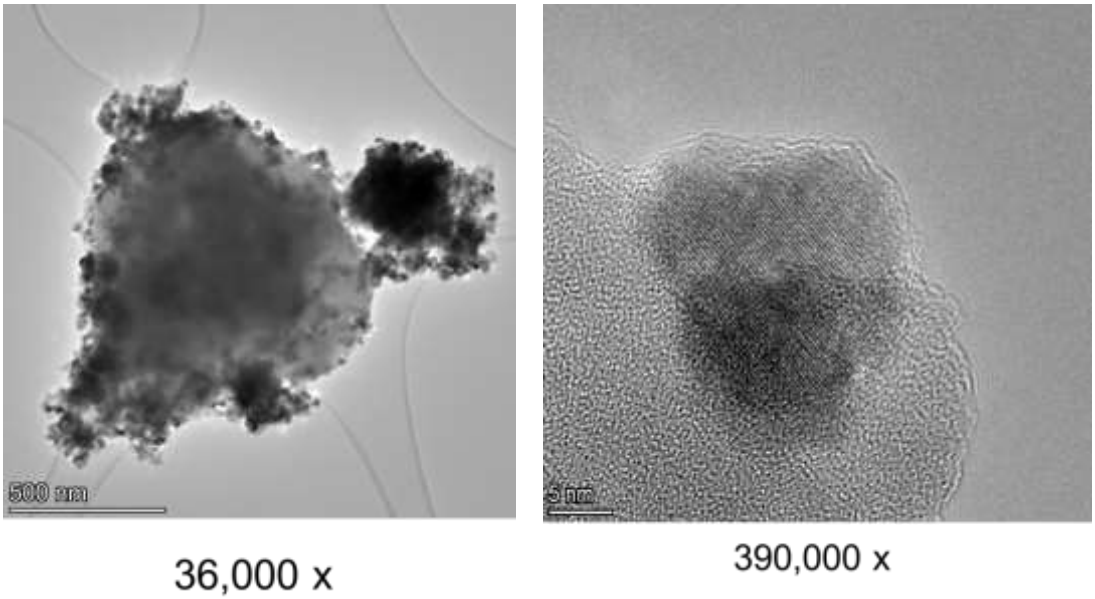

Figure 5 *– TEM images of Method 2 iron oxide nanoparticles on zeolite support.*

TEM imaging of the sample produced via the precipitation method, with no sodium content showed particles of a much more varied shape than those observed when synthesising by ionic liquid method 1. In the latter method, spherical particles only were produced whereas by precipitation, both spherical and elongated particles were isolated. These particles also showed an average particle size of 10-12 nm according to interpretation of the TEM imaging. Wei *et al.* reported a particle size of 13.1 nm, with a similar size and shape, the material produced via the precipitation method is comparable with that reported in literature.

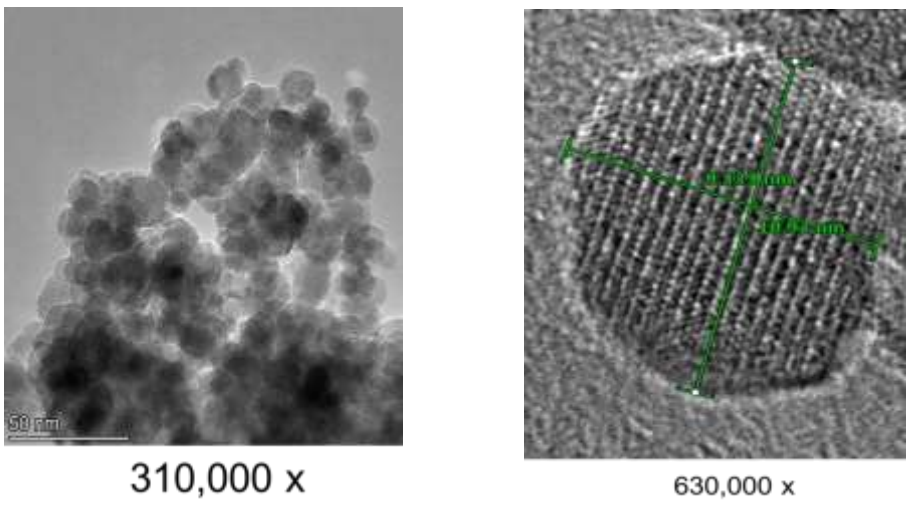

Figure 6 *– TEM imaging of Precipitation method no sodium content.*

Temperature-programmed reduction (TPR) is a widely used tool for the characterization of metal oxides dispersed on a support, in this case iron oxide on a zeolite support. The TPR method yields quantitative information of the reducibility of the oxide's surface, as well as the heterogeneity of the reducible surface.

TPR analysis has been carried out on each method of iron oxide synthesis in order to compare and contrast the reducibility of each catalyst. The TPR analysis for each type of precipitation method is shown in *Figure 7* below. The comparison of all methods is shown in *Figure 8* below.

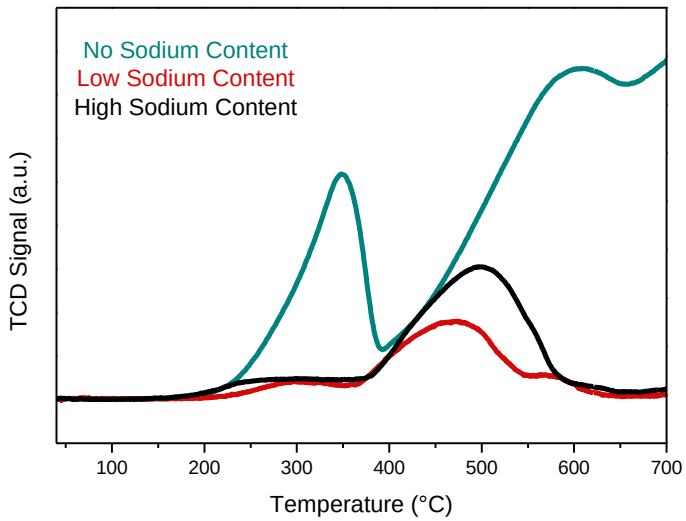

Figure 7 *- Showing TPR analysis for each precipitation method.*

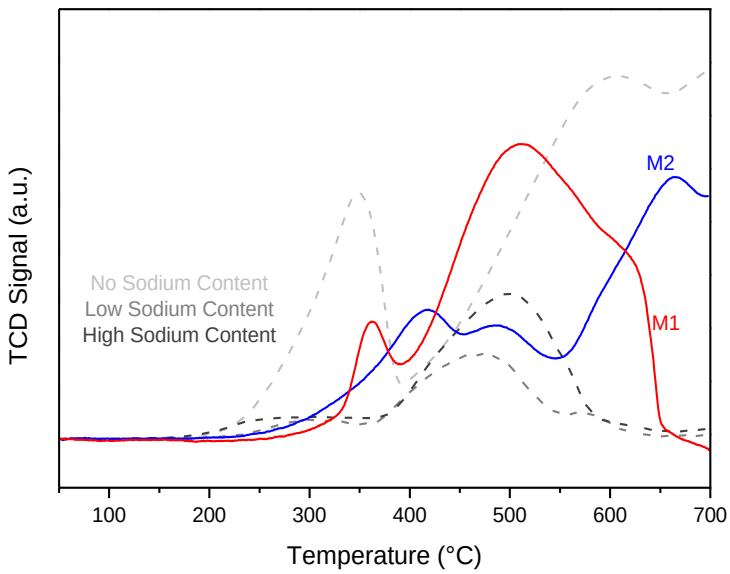

Figure 8 *– Shows TPR analysis for all methods*

Table 2 summarises the reduction temperatures and phases achieved by each method.

Method	*Calcined?*	*Temperature Fe_2O_3 -> Fe_3O_4*	*Temperature Fe_3O_4 -> FeO*	*Temperature FeO -> Fe*
1	*N*	*360°C*	*510°C*	*650°C*
2 – No NH_3	*N*	*410°C*	*510°C*	*693°C*
2 - No NH_3	*Y*	*416°C*	*500°C*	*663°C*
2 – With NH_3	*N*	*385°C*	*510°C*	*693°C*
2 – With NH_3	*Y*	*425°C*	*550°C*	*Reduction not completed*
PM – No Na	*N*	*347°C*	*588°C*	*Reduction not completed*
PM – Low Na	*N*	*300°C*	*480°C*	*Not observed*
PM – High Na	*N*	*250°C*	*500°C*	*Not observed*

***Table 2** - showing temperatures at which iron oxide reduces at each stage*

Figure 8 shows the TPR graphs obtained for each method together for a direct comparison of their hydrogen uptake and reduction temperature The most reducible of all the methods was, ionic liquid method 2 with NH_3 after calcination, as it had the largest area under the curve showing the greatest reducibility (Table 3). This is therefore the sample that would be expected to be the most active under reaction conditions when tested on the high-pressure rig, due to the need for the reduction of the iron oxide nanoparticles to the iron carbide as the active species for the Fischer-Tropsch synthesis, but that is yet to be confirmed.

Method	**Calcined?**	**Total Area Under the Curve (mV/min)**
1	N	0.74
2 – No NH_3	N	1.23
2 - No NH_3	Y	1.43
2 – With NH_3	N	1.38
2 – With NH_3	Y	**1.501**
PM – No Na	N	0.51
PM – Low Na	N	0.31
PM – High Na	N	0.52

Table 3 *– shows the total area under the curve as calculated from TPR analysis for all the samples prepared which relates to the amount of H_2 uptake by each catalyst.*

Conclusions and future work

In conclusion the precipitation method as described above has been successfully reproduced from literature and used as a comparison for the new methods introduced using ionic liquids. The method proposed by Wang et al. has been successfully prepared and compared with the novel method proposed herein at QUB. Method 2 proposed at QUB has been optimised producing much higher yields of >70% and is also a much less energy intensive method of producing the iron oxide nanoparticles. After TPR analysis it has been found that both ionic liquid methods show higher reducibility than the conventional precipitation method with method 2 showing the highest reducibility.

Future work will include the testing the activity of the catalyst in producing hydrocarbons of chain length C_5-C_{11} will be shown by use of a reactor for hydrogenation of CO_2 which is connected to a Gas Chromatograph (GC) with a specific column for detection of olefins in this chain length range. Recycling of the ionic liquid used in method 2 will also be attempted to achieve a more environmentally friendly synthesis. The pH of the reaction in method 2 will be closely monitored to optimise the morphology of the catalyst produced.

References

1. J. Wei, Q. Ge, R. Yao, Z. Wen, C. Fang, L. Guo, H. Xu and J. Sun, Nature Communications, 2017, 8, 15174.
2. Ce. Croopmémenittee, 2.
3. The Clean Power Plan, https://www.edf.org/clean-power-plan-resources, (accessed 12 March 2019) 2016, 290.
4. H. Yang, C. Zhang, P. Gao, H. Wang, X. Li, L. Zhong, W. Wei and Y. Sun, Catal. Sci. Technol., 2017, 7, 4580–4598.
5. I. Dimitriou, P. García-Gutiérrez, R. H. Elder, R. M. Cuéllar-Franca, A. Azapagic and R. W. K. Allen, Energy & Environmental Science, 2015, 8, 1775–1789.
6. M. D. Porosoff, B. Yan and J. G. Chen, Energy & Environmental Science, 2016, 9, 62–73.

QUILL Quarterly Report

August 2019 – October 2019

Name:	**Richard Woodfield**		
Supervisor(s):	Dr Stephen Glover, Dr Robert Watson and Prof Peter Nockemann		
Position:	PhD Student		
Start date:	13/06/2019	Anticipated end date:	13/12/2022
Funding body:	EPSRC		

Modelling the Use of Flow-Batteries in Transport Applications

Background

Lithium-ion cells are the current mainstream R&D candidate for energy storage in electric vehicles/hybrid electric vehicles (EVs/HEVs). Vanadium flow batteries have lower energy density per kilogram than these mainstream lithium-ion cells but the technology has not received the same intensive research and development over the past 20 years.

Flow-batteries are receiving a great deal of interest for transport applications in recent years due to having extremely long lifespans (up to 25+ years). Furthermore, the ability to simply refuel the cell in a similar manner to gasoline/diesel is very attractive, due to the energy being stored in liquid form. Range anxiety is a major issue with traditional battery electric vehicles, and if using flow batteries could become a realisation then there is potential to completely resolve this problem.
Very little work has been done in terms of investigating the feasibility of applying flow-batteries various types of transport. Identifying how much a flow-battery needs to improve by is extremely useful information for flow-battery chemists, for example.

This project focuses on investigation using vehicle modelling of new EV/HEV configurations which incorporate a flow-battery, for a range of transport applications. During the initial stages an assessment of the safety limitations of implementation into a vehicle will be conducted. The project may include the testing of flow batteries to generate input data, as well as identifying if certain conditions are viable for a flow-battery. One application may require a radically different design to another. The outcome should be to identify new transport applications for flow-batteries, which may include various types of hybridisation.

The project is sponsored by HORIBA MIRA, a world class vehicle proving grounds facility. The student will conduct a total of 6 months of work experience at the sponsor.

Objective of this work

- Assess safety limits/implications of implementing flow-batteries into transport
- Undertake flow-battery testing to gather data for models and validate intended applications
- To determine and rank key factors influencing performance
- Develop vehicle models to assess the viability of various configurations
- Quantify how much a flow-battery may need to improve by to meet the requirements of certain applications

- Undertake a full assessment of the future potential of flow batteries in EVs/HEVs

Progress to date

After spending some months on an industrial placement, the work done to date has been primarily focused on an early literature review.

Conclusions and future work

The literature shows some promise in certain transport applications for the successful implementation of a flow-battery through the use of modelling. An accurate flow-battery model will now be developed which will be modelled from the literature. This will form the starting point to insert the battery model into various vehicle models. Later work will involve experimental validation of flow battery performance to improve the accuracy of the models.